Fakultät für Physik und Astronomie

Ruprecht-Karls-Universität Heidelberg

Diplomarbeit

Im Studiengang Physik

vorgelegt von

Lea Gérard

aus Freiburg

2012

Spin-State-Selective Detection of Single Rubidium Atoms

Diplomarbeit

im Studiengang Diplom Physik
der Ruprecht-Karls Universität Heidelberg

angefertigt an der Fakultät für Physik
der Ludwig-Maximilians-Universität München
Lehrstuhl Prof. Dr. T. W. Hänsch

betreut durch Prof. Dr. H. Weinfurter

von

Lea Gérard

Erstgutachter: Prof. Dr. M. Oberthaler
Zweitgutachter: Prof. Dr. H. Weinfurter

Spezifischer Nachweis des Spinzustandes einzelner Rubidium Atome

Sowohl für Experimente der Grundlagenforschung als auch für Anwendungen der Quantenkommunikation und -information ist der Nachweis des spezifischen Spinzustandes von Atomen ein wichtiges Werkzeug.

Diese Diplomarbeit wurde an einem Experiment durchgeführt, das auf eine schlupflochfreie Überprüfung der Bell'schen Ungleichung hinarbeitet. In diesem Zusammenhang wird eine schnelle, zustandsabhängige Ionisation benötigt, die einen schnellen, zustandsspezifischen Nachweis einzelner ^{87}Rb Atome ermöglicht. Diese schnelle, effiziente Detektion ist eine wichtige Voraussetzung, um sowohl das Lokalitäts- als auch das Detektions-Schlupfloch zu schließen.

Es wird der Aufbau eines neuen gepulsten Diodenlasers bei 450 nm beschrieben, der potentiell eine schnellere Ionisation ermöglicht. Rechnungen zu einem möglicherweise schnelleren Detektionsschema werden erläutert und Ergebnisse von Messungen der Ionisationszeit für verschiedene Leistungen des Ionisationslasers werden dargestellt.

Im Experiment werden zwei verschränkte ^{87}Rb Atome in unterschiedlichen Aufbauten benutzt, um die Bell'sche Ungleichung zu testen. Der Verschränkte Zustand der beiden Atome wird in einem "Verschränkungs-Übertragungs-Prozess" aus zwei verschränkten Atom-Photon-Paaren hergestellt. Durch Kalibrierung der beiden Aufbauten konnte ein Kontrast der Atom-Photon-Verschränkung von über 90 % erzielt werden. Dies erlaubt, Verschränkung zwischen zwei Atomen mit einem Kontrast von über 0,707 zu erreichen. Dieser Wert ist notwendig ist, um die Bellsche Ungleichung zu verletzen.

Spin-State-Selective Detection of Single Rubidium Atoms

Efficient, state-selective detection of single atoms is an important tool both for experiments in fundamental physics as well as for applications in quantum communication and quantum information.

This thesis was done on an experiment towards a loophole-free test of Bell's inequality. Its violation would be an experimental proof against local hidden variable theories. In this context, an efficient, fast, state-selective ionisation is involved to enable an efficient sub-μs spin-state detection of single ^{87}Rb atoms, which is one important ingredient for closing both the locality and the detection loophole.

This thesis reports on the setup of a new pulsed diode laser of 450 nm to enable a faster ionisation process. It presents calculations of a potentially faster state read-out scheme as well as measurements of the ionisation time for different powers of the ionisation laser.

In the experiment, two remote entangled ^{87}Rb atoms in two different setups will be used to test Bell's inequality. This entanglement is generated in an entanglement swapping process using two entangled atom-photon pairs. By calibrating the two setups, a visibility of atom-photon entanglement above 0.90 was achieved. This allows the entanglement of remote atoms with a visibility above 0.707, which is necessary to violate Bell's inequality.

Contents

1 Introduction

Efficient state detection of single atoms is an important tool not only in experiments in the field of atomic physics and quantum optics, but also for applications in quantum information and quantum communication. Single atoms can be cooled and trapped by standard techniques (see e.g. [1]) and their internal states can be addressed and manipulated. Using specific preparation and detection techniques, it is possible to encode a qubit in the atomic state. A qubit is a quantum system which can have two binary measurement results (1 and 0), but unlike a classical bit, the qubit can be in a state of a superposition of the two eigenstates $|0\rangle$ and $|1\rangle$ and several qubits can be entangled and consequently show non-classical correlations in their measurement results. Qubits can be used for example as quantum memories, nodes in quantum repeaters, or in quantum cryptography. They also find interesting applications for the study of fundamental physics, e.g. quantum simulations in optical lattices.

Ionisation presents a technique to efficiently detect the Zeeman-state of an atom with a high spatial resolution. Together with an efficient method to detect the ionisation fragments, the detection time of an atom can be reduced to less than 1 μs. In future, state selective ionisation together with a detection of the fragments by channel electron multipliers [2] might be used for site specific read-out of the state of atoms in optical lattices [3, 4, 5, 6, 7].

The fast, state-selective detection of single atoms is also an important ingredient for a future loophole free test of Bell's inequality using two remote entangled ^{87}Rb atoms. While the efficiency of the detection of atoms is close to one, closing the detection loophole, a spacelike separation of the state measurements of the two atoms has to be achieved by a fast state read-out.

Overview

This thesis starts with a description of the already existing experiment which consists of two setups, each of them containing a single atom entangled with an emitted photon. The two single atoms are entangled via entanglement swapping by a Bell state measurement on the two emitted photons. This pair of remote entangled atoms could enable a future loophole-free test of Bell's inequality, making spin-state measurements on the atoms. Preparations of the setups for atom-atom entanglement are explained with the main goal of improving the fidelity of the atom-photon entanglement as well as the synchronisation and connection of the two setups. This enables entanglement between remote atoms with a visibility over 0.707, the value which is necessary to violate Bell's inequality.

The second part is about spin-state-selective detection of ^{87}Rb atoms by ionisation. A potentially faster ionisation scheme is presented, and calculations on detection efficiencies and the needed time are carried out. Following this is a description of the setup of a pulsed diode laser at 450 ns, which can be used for ionisation. In this thesis two different laser diodes are tested in order to achieve the highest power possible for ionisation in our experiment. In the end, results of the measurements of the ionisation times, which are measured after the newly set up laser has been integrated into the main experiment, are presented.

2 Description of the main Experiment

This chapter gives an overview of the main experiment. The idea of a Bell-test is presented and a brief description of entanglement is given before the setup is described.

2.1 Introduction and long term Goal

In 1935 Einstein, Podolsky and Rosen wrote their famous paper: "Can Quantum-Mechanical Description of Physical Reality Be Considered Complete?"(EPR-paper) [8] in which they question the completeness of quantum mechanics. Under the assumptions that *reality* does not depend on the the measurement and that two spacelike separated events do not influence each other (*locality*), they concluded that quantum mechanics cannot give a complete description of nature: In their gedankenexperiment, Einstein et al. describe two particles which are entangled [1] in their momentum and position degree of freedom. By making either position or momentum measurements on the second particle, one could infer either the position or the momentum of the first particle meaning that both quantities belong to the same reality. However, according to Heisenberg's uncertainty principle, momentum and position cannot be predicted with probability of one at the same time and therefore cannot be part of the same reality. This leads to the conclusion of quantum mechanics not being a complete theory. To solve this problem, the authors proposed to introduce parameters which are hidden to the experimentalist to complete the theory. Such theories were later called local hidden variable (LHV) theories. The question of quantum mechanics being complete or not was philosophical until 1964 when Bell found an inequality [10] which gives an upper bound for statistics on correlation measurements on

---

[1]In the EPR-paper the term "entangled" - which was later introduced later by Schrödinger [9] - was not used, but they thought of two particles that are separated after having interacted, but still have to be described by a common wave function.

two spin-$\frac{1}{2}$-particles. In the CHSH formulation [11], Bell's inequality reads:

$$S(\vec{a}, \vec{b}, \vec{a}', \vec{b}') := |\langle \sigma_{\vec{a}} \, \sigma_{\vec{b}} \rangle - \langle \sigma_{\vec{a}} \, \sigma_{\vec{b}'} \rangle| + |\langle \sigma_{\vec{a}'} \, \sigma_{\vec{b}} \rangle + \langle \sigma_{\vec{a}'} \, \sigma_{\vec{b}'} \rangle| \leq 2 \qquad (2.1)$$

where $\sigma_{\vec{a}}$ and $\sigma_{\vec{a}'}$ ($\sigma_{\vec{b}}$ and $\sigma_{\vec{b}'}$) are spin measurements performed on the first (the second) particle in direction $\vec{a}$ or $\vec{a}'$ ($\vec{b}$ or $\vec{b}'$). Quantum mechanical results exceed the upper bound of 2 for certain angles. This shows that LHV theories and quantum mechanics are not compatible and offers a method to experimentally rule out LHV theories. Several experiments have been performed [12, 13, 14, 15, 16, 17, 18], all of them confirming quantum mechanics. However, two problems appear which so far could not be solved both in the the same experiment:

One is, that one has to make sure that the information about the measurement made on one particle does not influence the outcome of the measurement on the second particle (*locality loophole*). The other problem is an inefficient detection (*detection loophole*) [19, 20]. The long term aim of our experiment is to perform a test of Bell's inequality with two entangled atoms which are separated by approx. 300 m. The use of atoms allows a detection efficiency of close to one and the distance allows for a detection time of $t = \frac{300m}{c} \approx 1\mu$s.

2.2 Entanglement

Entanglement is one of the most striking features of quantum mechanics. By making measurements on two entangled particles which can be separated by arbitrary large distances, one can observe correlations which cannot be explained by classical statistics.

Definition of Entanglement

Two (or more) particles are entangled if their state cannot be written as a tensor product:

$$|\Psi\rangle_{12} \neq |\Psi\rangle_1 \otimes |\Psi\rangle_2 \qquad (2.2)$$

Bell States

For a two qubits system, one can define a basis consisting of four maximally entangled states. These states are called Bell states and are defined as follows:

$$\left|\Psi^-\right\rangle = \frac{1}{\sqrt{2}}(\left|\uparrow\right\rangle\left|\downarrow\right\rangle - \left|\downarrow\right\rangle\left|\uparrow\right\rangle)$$

$$\left|\Psi^+\right\rangle = \frac{1}{\sqrt{2}}(\left|\uparrow\right\rangle\left|\downarrow\right\rangle + \left|\downarrow\right\rangle\left|\uparrow\right\rangle)$$

$$\left|\Phi^-\right\rangle = \frac{1}{\sqrt{2}}(\left|\uparrow\right\rangle\left|\uparrow\right\rangle - \left|\downarrow\right\rangle\left|\downarrow\right\rangle) \tag{2.3}$$

$$\left|\Phi^+\right\rangle = \frac{1}{\sqrt{2}}(\left|\uparrow\right\rangle\left|\uparrow\right\rangle + \left|\downarrow\right\rangle\left|\downarrow\right\rangle)$$

where $\{\left|\uparrow\right\rangle, \left|\downarrow\right\rangle\}$ is the basis for each qubit.

Properties of entangled States

Entanglement does not depend on the measurement basis and cannot be created or destroyed by local unitary operations. For two entangled particles, the measurement outcomes are correlated in any measurement basis.

2.2.1 Entanglement Swapping

There are different schemes to entangle two particles, generally involving interaction between them. Entanglement swapping provides, however, a method to entangle two particles that have never interacted [21]. In order to perform an entanglement swapping process, two pairs of entangled particles are necessary. Particle 1 and 2 are entangled and particle 3 and 4 also. The aim is now to entangle e.g. particle 1 and 4. This can be done by making a Bell-state measurement, i.e. a projection on a Bell state, of particle 2 and 3 (see fig. 2.1). Let's assume the two pairs of particles are in state $\left|\Psi^-\right\rangle$ each:

$$\begin{aligned}
\left|\Psi\right\rangle_{1234} &= \left|\Psi_{12}^-\right\rangle \otimes \left|\Psi_{34}^-\right\rangle \\
&= \frac{1}{2}(\left|\Psi^-\right\rangle_{14} \otimes \left|\Psi^-\right\rangle_{23} + \left|\Psi^+\right\rangle_{14} \otimes \left|\Psi^+\right\rangle_{23} \\
&\quad + \left|\Phi^-\right\rangle_{14} \otimes \left|\Phi^-\right\rangle_{23} + \left|\Phi^+\right\rangle_{14} \otimes \left|\Phi^+\right\rangle_{23})
\end{aligned} \tag{2.4}$$
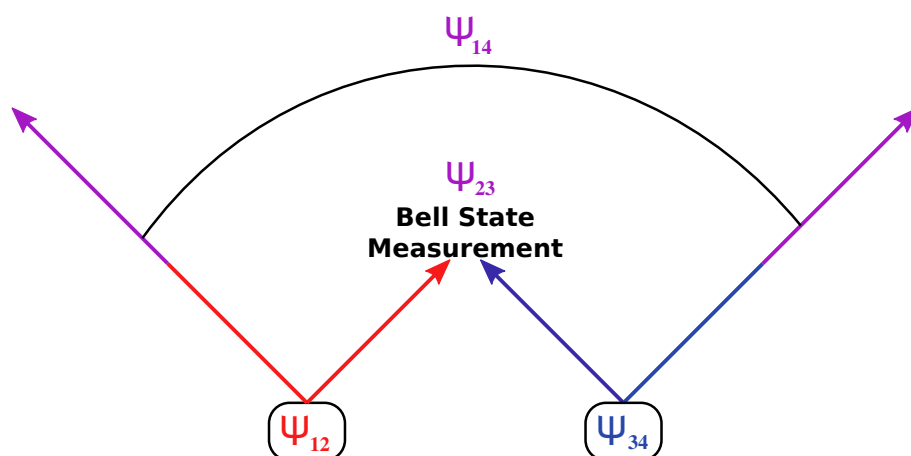
Figure 2.1: Entanglement swapping

Here one can easily see that when one measures a Bell-state of particle 2 and 3, particle 1 and 4 are projected into the same Bell-state.

2.3 The Experimental Setup

The experiment aims at entangling two remote atoms in order to enable a future loophole-free test of Bell's inequality. The use of atoms makes it possible to obtain a detection efficiency close to one. Each of the atoms is entangled with a spontaneously emitted photon. The two atoms are then entangled by entanglement swapping (see section above). It is possible to guide photons in an optical fibre over a large distance which will allow to separate the two atoms by approx. 300 m and it should be possible to close the locality loophole by performing fast and efficient measurements on these atoms [22]. This idea is implemented as follows:

There are two atom traps in different laboratories. An overview of these setups is shown in fig. 2.2. In each of them, a single ^{87}Rb atom is trapped in an optical dipole trap (ODT) which is loaded from a magneto-optical trap (MOT) [1]. The MOT provides cooling for the atoms. The ODTs are generated by a tightly focussed Gaussian beams of far red detuned light with a waist of 3.5 μm and 1.9 μm respectively. This small waist ensures that
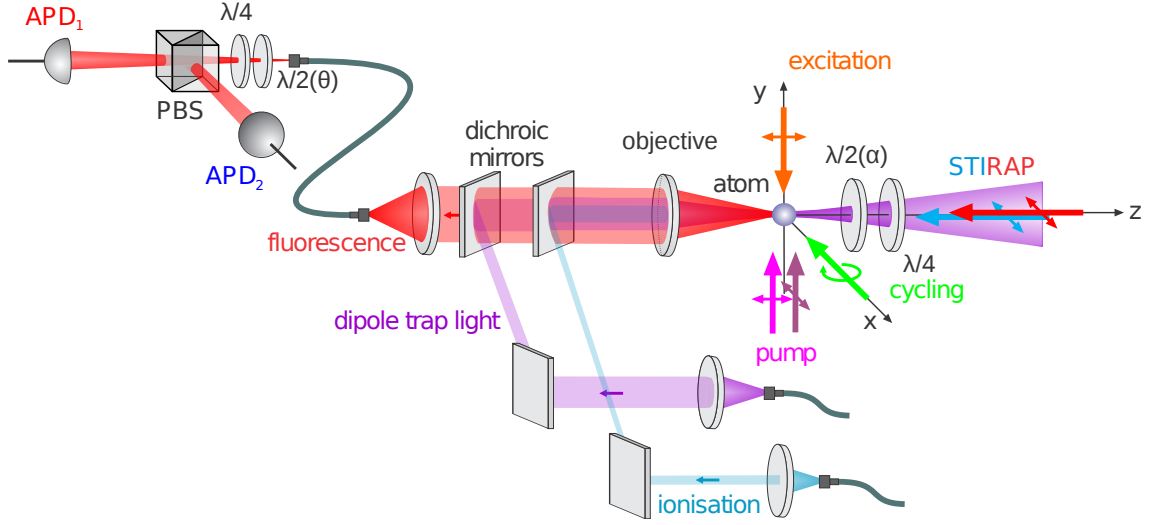
Figure 2.2: Schematic of the atomic trap with the lasers used for generation of entangle-
ment and for detection. Additionally, the two avalanche photodiodes (APDs)
are depicted. They collect the flourescence light behind the polarizing beam
splitter (PBS).

there is only one single atom trapped at once. The loading of a second atom in the ODT
leads to two body collisions [23] producing the loss of both atoms.

In each of the traps, an atom can be entangled with a spontaneously emitted photon
(see below). The two traps are connected by an optical fibre which guides the photon
emitted in one setup to the other one where a Bell-state-measurement of the two photons
is performed (see fig. 2.3). At the moment, the two setups are 20 m apart from each other,
but it is planned to separate them by approx. 300 m. This will give us the time us 1
$\mu s \approx 300 \, m \cdot c$ to perform the measurements of the atoms' states.

2.3.1 ^{87}Rb and the Laser System

The atom used for the experiment is ^{87}Rb . It is an alkali metal which means that it has
one valence electron. Therefore, the energy spectrum is hydrogen-like. Its nuclear spin is
$I = \frac{3}{2}$, which leads to the two hyperfine states F = 1, 2 for $j = \frac{1}{2}$, and to the four hyperfine
states F = 0, 1, 2, 3 for $j = \frac{3}{2}$ (see fig. 2.4).
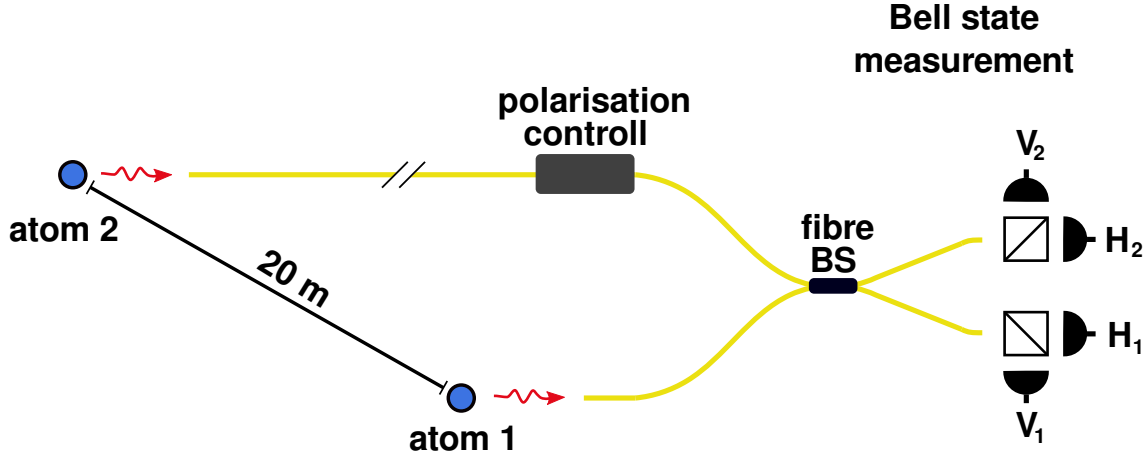
Figure 2.3: The two atomic traps are connected by an optical fibre. The emitted photons are guided to a fibre beam splitter where they interfere. Afterwards the polarisation is analysed by means of PBS and detected by four APDs.

The atom's ground state is the $5^2S_{1/2}$ state and the two first excited states are $5^2P_{1/2}$ (D_1 line, 795 nm) and $5^2P_{3/2}$ (D_2 line, 780 nm) (see fig. 2.4). The wavelengths of these two transitions are in the near infrared and are accessible by commercial diode lasers.

In this experiment, six diode lasers are used, two of them at 780 nm, two at 795 nm, one at 856 nm and one at 450 nm. The last one is used for ionisation, and its setup is described in chapter 5. The other lasers are locked to atomic transitions. In order to address the chosen Zeemam- and hyperfine states, the laser frequencies can be shifted by acousto-optic-modulator (AOM) [24]. At the same time, AOMs can be used to control the light intensity and for forming pulses of desired temporal shape. The laser sequences are controlled by a programmable pattern generator with a time resolution of 20 ns. Image 2.4 gives an overview of the laser system.
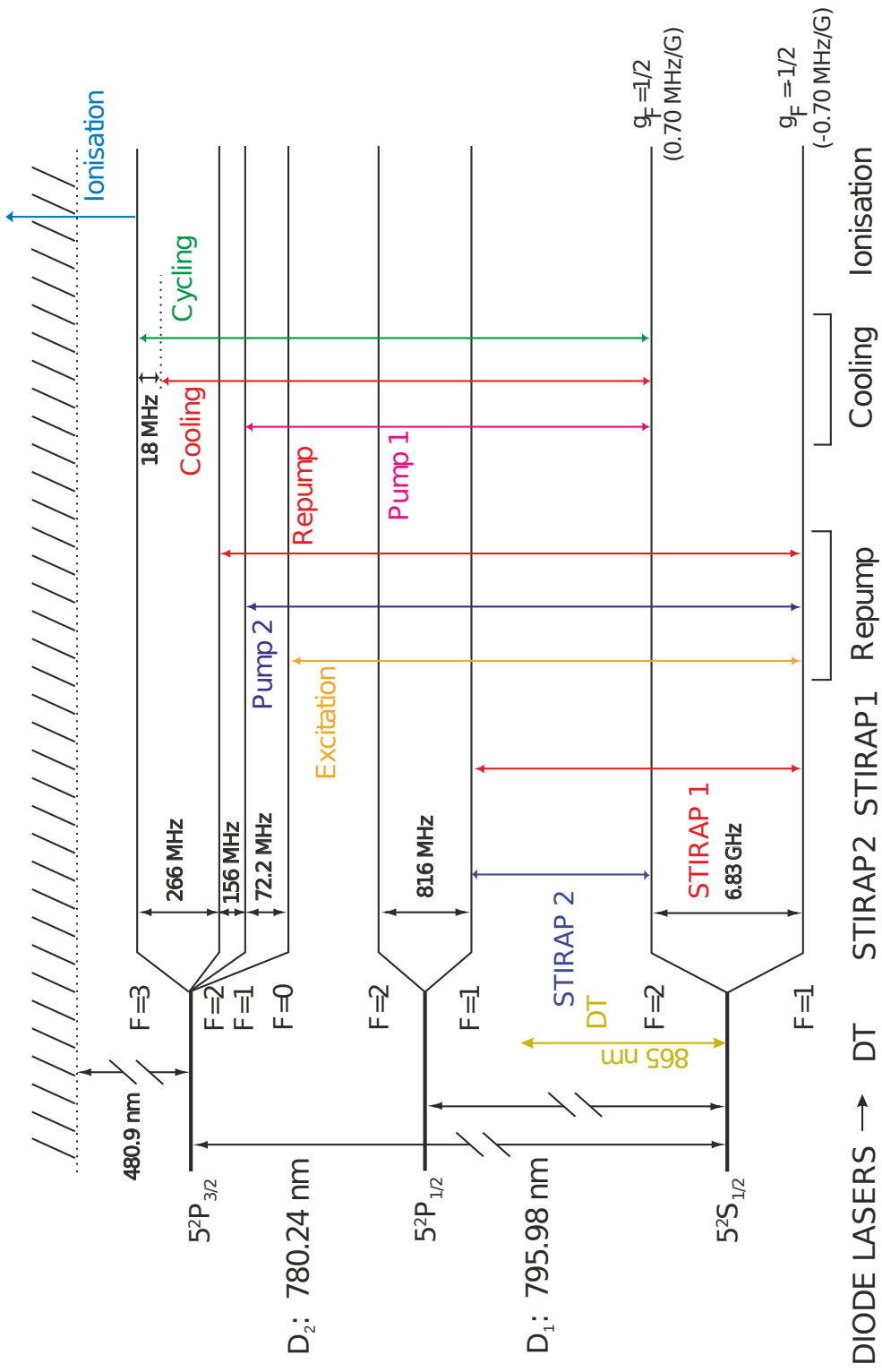
Figure 2.4: The laser system used in our experiment.

2.4 Generation of Atom-Photon-Entanglement

Atom-photon entanglement is generated in a spontaneous decay from the $5^2P_{3/2}$, F' = 0, $m_F = 0$ state to $5^2S_{1/2}$, $F = 1$, $m_F = 0$ (D$_2$-transition) [25, 26]. The initial state $5^2S_{1/2}$, $F = 1, m_F = 0$ is prepared by optically pumping the atom with the lasers pump1 (pink, see fig. 2.5, A), pump2 (violet) and the cooling laser (red). From this state, a π-pulse is applied using the excitation laser (orange) that excites the atom to the state $5^2P_{3/2}$, $F' = 0$, $m_F = 0$. Once it is excited, there are three possible decay channels: The atom can spontaneously decay into the $m_F = -1$, $m_F = 0$ or $m_F = +1$ Zeeman-state of the $5^2S_{1/2}$, $F = 1$ ground state (see fig. 2.5, B). The emitted photon is collected by an optical fibre which does not couple the π-polarised light, therefore only σ-polarized light is transmitted [27]. In our case, the spontaneous emission is a coherent process, as the whole system of atom *and photon* is considered. The Zeeman state of the atom is correlated with the polarisation of the photon: If one observes the Zeeman state $m_F = +1$ ($m_F = -1$) the photon is σ^- (σ^+) polarised. This yields the entangled state:

$$|\Psi\rangle_{Ap} = \frac{1}{\sqrt{2}}(|1,-1\rangle_z |\sigma^+\rangle_z + |1,+1\rangle_z |\sigma^-\rangle_z) \tag{2.5}$$

Figure 2.5: Generation of atom-photon entanglement

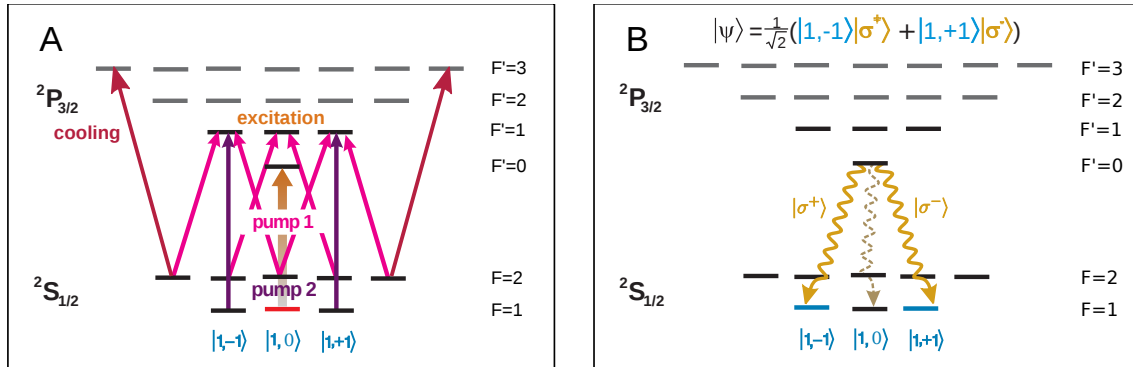## 2.5 Verification of Atom-Photon-Entanglement

In order to verify the entanglement one has to measure correlations between the polarisation of the photon and the spin state of the atom. This has to be done in at least two conjugate bases, e.g. (H/V) and (±45°), to make sure that the correlations are not of classical nature.

Detection of the Photons

The emitted photon is guided to a polarising beam splitter (PBS) and then detected by avalanche photo diodes (APDs) which are located at each output port of the PBS (see fig. 2.2). A $\lambda/2$ and a $\lambda/4$ wave plate in front of the PBS allow to select the basis of this measurement.

2.5.1 Atom State Read-out

The aim is to project the atom on a selected superposition of $m_F = \pm 1$ of the $F = 1$ ground state. For this purpose, the chosen superposition is first transferred to the $F = 2$ state of the ground state. From there it is excited by the cycling-laser (see fig. 2.4) to the $5^2P_{3/2}$, $F' = 3$ state. Then it can be ionised by the ionisation laser in order to remove the atom from the trap. Whether the atom is still in the trap can be determined by the fluorescence level of the cooling light. In order to make the detection faster, Channel Electron Multiplier (CEMs) can be installed [2]. A schematic of the detection process is given in fig. 2.6

STIRAP

STIRAP is an abbreviation for "stimulated Raman adiabatic passage" and describes the process of transferring the population of one state, here $F = 1$ of the ground state to a second one, here $F = 2$ of the ground state by a sequence of two consecutive laser pulses, with the Rabi frequencies Ω_1 and Ω_2 which couple to a third excited level [28]. The transfer can ideally have an efficiency of 100 %.
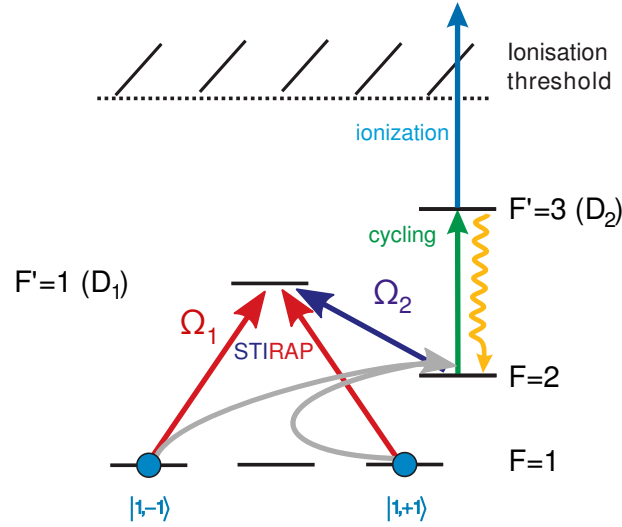
Figure 2.6: STIRAP transition and subsequent ionisation for spin-state detection of the atom.

The selection rules of atomic transitions permit to select a "bright state" which couples to Ω_1 and a "dark state" which does not by choosing a superposition of σ^+ and σ^- light [29]. Only the bright state is transferred. A detailed description of the STIRAP process is given in section 4.3.1.

Ionisation

An atom, which has been transferred to $F = 2$ can be excited by the cycling laser to the $5^2P_{3/2}$, $F' = 3$ level. From there it can be ionised with the ionisation laser. The cycling laser is operated at several hundred times the saturation intensity so that several Rabi cycles are driven during one pulse and it can be assumed that the population of the excited state is close to $\frac{1}{2}$. A different scheme for the detection by ionisation which does not require a STIRAP transition is possible. In this scheme, the atom is optically pumped to the $5^2P_{1/2}$, $F' = 1$ and directly ionised from there (see chapter 4).

2.6 Atom-Atom-Entanglement

In order to generate entanglement between two remote atoms, a Bell-state-measurement on the two photons emitted by the single trapped atoms has to be carried out (see section 2.2.1). For this purpose, the photon of the setup 2 is guided to the setup 1 where the Bell-state analyser is situated (see fig. 2.3). It consists of a fibre beam splitter (BS), a PBS in each output port and four APDs after the two PBS.

Two Photon Interference at a Beam Splitter

A Bell-state measurement on the two photons means, that the photons are projected onto a maximally entangled state. For the polarisation degree of freedom, this is achieved as follows: As photons are bosons, the total wave function has to be symmetric. This means, if the state is even (odd) under interchange of the two photons, also the spatial part of the wave function has to be even (odd). Since $|\Psi^-\rangle$ is the only of the four Bell-sates which is odd under permutation of the two photons, it is the only state for which the two photons leave the fibre BS at different output ports (see also [30]) and can therefore be unambiguously detected by coincidences V_1H_2 or V_2H_1 (see fig. 2.3). Since it is desirable to detect more than one of the four possible Bell-states, PBS are placed in the output ports of the fibre BS. This allows to detect also $|\Psi^+\rangle$ by a coincidence V_1H_1 or V_2H_2. The states $|\Phi^-\rangle$ and $|\Phi^+\rangle$ lead both to V_1V_1, V_2V_2, H_1H_1 or H_2H_2 which are different to $|\Psi^-\rangle$ and $|\Psi^+\rangle$, but cannot be distinguished from each other. This means, the Bell-state projection succeeds in 50 % of the cases. It is an important feature that one obtains a signal every time when the preparation of an entangled pair has been successful (heralding).

Verification of Atom-Atom Entanglement

In order to verify the entanglement of the atoms, correlations in two bases are measured. The bases here are chosen by two different STIRAP polarizations of one setup and like in the correlation measurement of atom-photon-correlations, the polarisation of the STIRAP of the other setup is varied. With this methods entanglement has been verified.

2.7 Fast and efficient Ionisation in the Context of this Experiment

One of the main goals of this experiment is to perform a loophole-free test of Bell's inequality. While detection with efficiency close to one is necessary in order to close the detection loophole, a spacelike separation of the measurements on the atoms has to be achieved in order to close the locality loophole. The time which is needed for the state analysis of the atoms has to stay below $t_{meas} < \frac{d}{c}$, where d is the distance between the two traps and c the speed of light. In order to keep the distance of the two setups as small as possible to avoid losses in the optical fibre, the state analysis has to be as fast as possible. The aim is to separate the two atom traps by 300 m which gives 1 μs for measurement. In this time, the state of the atom does not only have to be efficiently detected, but also the measurement basis has to be randomly chosen and set by an EOM (random setting of measurement basis: 100 ns [22, 31]). If Channel Electron Multipliers are installed, which can detect the ionisation fragments within a time inferior to 500 ns [2], the state selective ionisation process has to be finished within 400 ns.

3 Towards Atom-Atom Entanglement

In order to violate Bell's inequality with two remote entangled atoms, the visibility of their entanglement has to exceed 0.707 [19]. When creating this remote entanglement via entanglement swapping, two highly entangled atom-photon pairs are required. A high fidelity entanglement is also necessary for the verification of the atomic state read-out scheme presented in chapter 4 as the entanglement is a way to prepare superpositions of the $F = 1$, $m_F = \pm 1$ states of the ground state, which serve as initial states in the read-out process.

In this chapter, calibration measurements are described with the main aim of improving the visibility of the atom-photon entanglement as well as the connection and the synchronisation of the excitation procedures of the two setups, which is essential for the entanglement of two atoms.

3.1 Compensation of Magnetic Fields

In a magnetic filed, the energy of the Zeeman states is shifted by: $\Delta E_{Zeeman} = -\vec{\mu}\vec{B}$ (Zeeman-effect) with $\mu = \mu_B g_F m_F$ being the magnetic moment where $\mu_B = \frac{e}{2m_e}\hbar = 2\pi\hbar \cdot 1.4 MHz/G$ is Bohr's magnetron and g_F the Landé factor which is equal to $-\frac{1}{2}$ here. The spin-state of the atom therefore undergoes precessions in a magnetic field. The magnetic fields have to be compensated in a way that the evolution is slow enough so that the spin state does not change before it is detected. Another problem of the Zeeman-splitting is, that the degeneracy of the two states $|1, -1\rangle$ and $|1, +1\rangle$ of our qubit is lifted. This could lead to a distinguishability of the spontaneously emitted photons. However, typical fields on the order of milligauss cause frequency shifts on the order of kilohertz. This is small compared to the natural linewidth of 6 MHz so that this energy shift does neither affect

the entanglement, nor the interference of the two spontaneously emitted photons from the different setups.

In our experiments, there are magnetic disturbances coming from electric devices and from the strong current of the nearby subway. These fluctuations are on the order of 20-30 mG [32, 33].

3.1.1 Description of a Spin-1-System in a Magnetic Field

The Hamiltonian describing the interaction of a spin of one with a magnetic field is given by [32]:

$$\mathcal{H} = \vec{B}_{eff} \frac{\mu_B \, g_F}{\hbar} \vec{\mathcal{F}} \tag{3.1}$$

where $\vec{\mathcal{F}}$ is the angular momentum operator for spin equal to one.

Let the eigenstates of the interaction Hamiltonian be $|\Phi_0\rangle$, $|\Phi_+\rangle$ and $|\Phi_-\rangle$. The time evolution of an arbitrary state $|\Psi(0)\rangle = c_{+1} |\Phi_+\rangle + c_0 |\Phi_0\rangle + c_{-1} |\Phi_-\rangle$ is given by:

$$|\Psi(t)\rangle = c_{+1} |\Phi_+\rangle \, e^{-i\omega_L t} + c_0 |\Phi_0\rangle + c_{-1} |\Phi_-\rangle \, e^{i\omega_L t} \tag{3.2}$$

This means, the state evolves periodically with the Larmor frequency ω_L.

The definition of the Larmor frequency gives the relation between the evolution frequency and the strength of the magnetic field:

$$f = \frac{\omega_L}{2\pi} = \frac{\mu_B \, g_F}{2\pi\hbar} B_{eff} = 700 \frac{Hz}{mG} \cdot B_{eff} \tag{3.3}$$

where $\mu_B = 2\pi\hbar \cdot 1.4 MHz/G$ was used.

A typical residual field after compensation is of some milligauss which corresponds to a Larmor period of some hundred microseconds. As the state read-out is completed within $10\,\mu$s, this level of compensation is sufficient.

Effects of the Spin-State Precession on the State Detection of our Qubit

The state read-out of our qubit is a projection on the dark state (with respect to STIRAP 1). An initial spin-state of the atom evolves in time due to the magnetic fields, and therefore its projection onto the dark states will also evolve. This means that the state read-out after a certain waiting time t will not give the original state projection.

If a magnetic filed is applied along the quantisation axis (here z-axis), the evolution of the dark and the bright state takes place only in the space of our two qubit states, i.e. $|\Phi_0\rangle$ which is here equal to $|1,0\rangle$ is not involved. In general, however, the evolution contains the state $|1,0\rangle$.

Consider a magnetic field such that the dark state is an eigenstate of the Hamiltonian (i.e. does not evolve) and the initial bright state oscillates between the bright state and $|1,0\rangle$. Since $|1,0\rangle$ is not detected it is also a bright state and precessions between two bright states cannot be observed.

In a case of a guiding field, i.e. if the magnetic field in one direction is several times stronger than in the other directions, the state is stable in one basis and it seems as if there is no magnetic field, while fast oscillations can be seen when measuring in the conjugate basis.

The last two examples above demonstrate the need to make the measurements of the evolution of the spin-state in two bases.

3.1.2 Experimental Implementation

Correction of magnetic fields

In order to be able to control the magnetic field, three pairs of compensation coils are installed around the trap. A magnetic field sensor is mounted outside the vacuum glass cell close to the position of the ODT. It provides three voltage values which are proportional to the magnetic fields in the three spatial directions, up to a sensor-specific offset. The

fields are stabilised by a feedback-loop using those values . Due to the offset of the sensor and also because it cannot be installed at the position of the atom is, the set values have to be determined experimentally by measuring the temporal evolution of the atomic state.

Measurements of the Temporal Evolution of the Spin-States

In a measurement, the projection on the dark state is measured in a basis chosen by the polarisation of the STIRAP 1 laser (see section 2.5.1). This is done by transferring the bright state to the $F = 2$ state of the ground state by the STIRAP and then ionising the atom. After this procedure, the fluorescence level of the cooling light indicates if the atom is still in the trap. While an atom in the dark state should still be in the trap, the bright state is removed. This procedure is repeated several hundred to several ten thousand times with single atoms.

In order to make the temporal evolution of the spin-state visible, this projection on the dark state is done varying the waiting time before the state is read-out.

Usually, different magnetic fields can cause similar frequency patterns and therefore, several iterations are necessary to determine the right voltage values. Furthermore, the ODT causes an effect similar to magnetic fields due to circular polarisation which is caused by the birefringence of the vacuum glass cell [32].

Therefore, the procedure is to first measure with the dipole trap turned off and trying to optimize the set voltage value in z-direction, i.e. minimize the B-field in z-axis (which is chosen as the quantisation axis). After this, one can turn on the dipole trap again because all the effects in z-direction should now be caused by the circular polarization of the light. By rotating the linear polarisation of the dipole trap, this part caused by the light can be minimised. Magnetic fields in x- and y-direction are also compensated.

Figure 3.1 shows an example of state evolution before and after compensation. Before compensation, the Larmor frequency was about 50 kHz which would lead to significant errors in the state detection. After the compensation, the period of a Larmor precession was well above $200 \, \mu$s so that a state read-out within the first $10 \, \mu$s is practically not influenced by the remaining magnetic fields. When projecting the atom on $\frac{1}{\sqrt{2}}(|1, +1\rangle +$
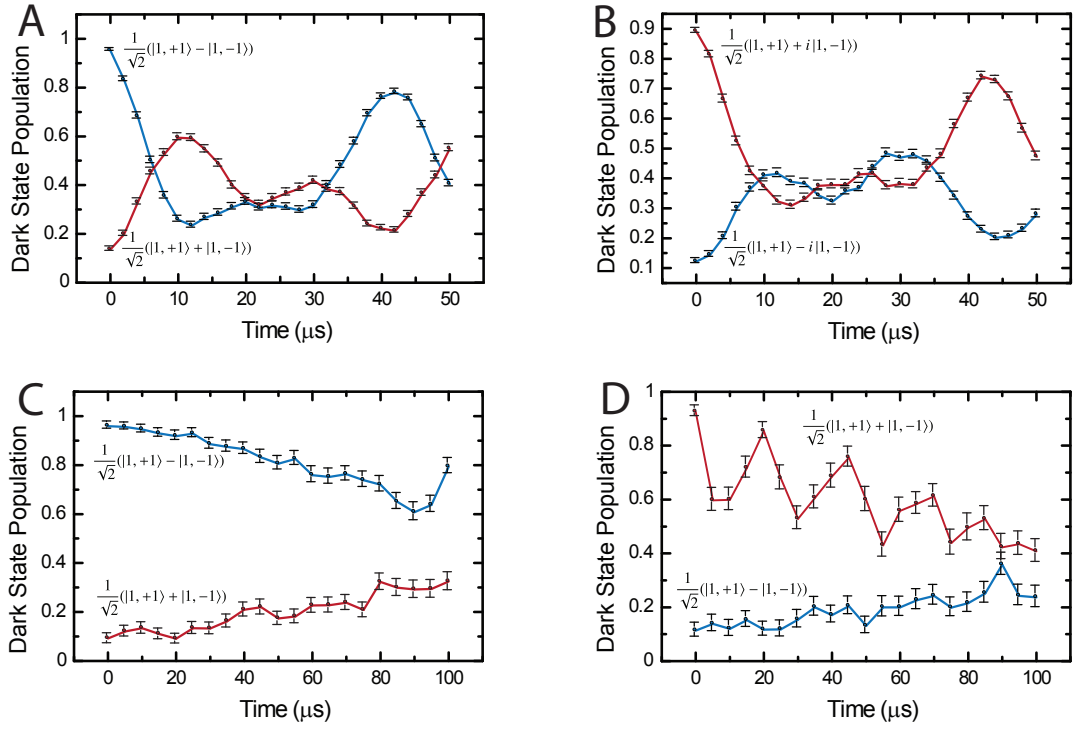
Figure 3.1: Larmor precession of the dark and the bright state. The atom is projected on $\frac{1}{\sqrt{2}}(|1,+1\rangle - |1,-1\rangle)$ (A, C), $\frac{1}{\sqrt{2}}(|1,+1\rangle + i\,|1,-1\rangle)$ (B) and $\frac{1}{\sqrt{2}}(|1,+1\rangle + |1,-1\rangle)$ (D), respectively. A and B was measured before the compensation and C and D afterwards. The residual oscillation in D is due to the dipole trap and not caused by magnetic fields.

$|1,-1\rangle)$, there is a residual oscillation of the dark state which is due to effects of the dipole trap [32] and not because of magnetic fields.

3.2 Polarisation Errors of the STIRAP

Polarisation Standard for both Setups

In order to achieve high fidelity entanglement between photon and atom as well as between two atoms, it is important that the polarisation of the atomic analysis basis and

the photon detection basis coincide. For this reason, a set of mounted polarisers[1] was set up which defines the polarisation axes in our two setups. Their orientation is never changed and they are used in both setups. The extinction ratio for the polarisers used is 1:10 000.

3.2.1 Polarisation Errors due to Mirrors

When light is reflected by a mirror, the polarisation parallel (P) and orthogonal (S) to the incidence plain stay the same, but a relative phase between them is introduced [34]. Therefore, all the other polarisations, which are a superposition of P and S, are changed. In our setup P coincides with the horizontal polarisation (H) and S with vertical polarisation (V) with respect to the surface of the optical table. The polarisations of $\pm 45°$ are consequently changed due to the phase shift. For dielectric mirrors, this effect is stronger than for silver mirrors and it is also temperature dependent and therewith time dependent. Therefore, the dielectric mirrors were exchanged for silver mirrors. There is still a phase between H and V, but it is temporally constant.

3.2.2 Experimental Procedure to Adjust the Polarisation

In order to compensate for the introduced phase which occurs at the mirrors, a wave plate is used. The eigen-axes are aligned parallel to H and V so that light of these polarisations is not changed when passing. By tilting the plate, one can induce another, selectable phase between H and V as one changes the length of the path of those beams through the wave plate. This phase can compensate the effects of the mirrors on the $\pm 45°$ polarisation (and any other superposition of H/V).

A pre-compensation of this phase is done by minimising the extinction ratio in a configuration where one of two crossed polarisers is placed after the optical fibre and the second one after the vacuum glass cell where the atoms are trapped (see fig. 3.2). An extinction ratio of 0.23 % ($\pm 45°$) and 0.01 % (H/V) was achieved.

The birefringence of the vacuum glass cell is an additional problem here as it introduces

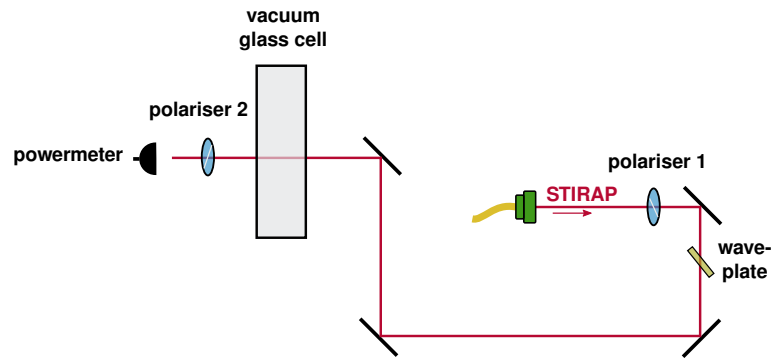---

[1]thin film polarisers by codixx

Figure 3.2: Setting for the pre-compensation of the phase shift introduced by reflections at the mirrors.

circular polarisation. Furthermore, the polarisation cannot be measured at the position of the atom within the cell. Therefore one expects errors in the state-detection which are due to changes in the polarisation when the STIRAP beam enters the glass cell.

A method to detect polarisation errors at the atom is as follows: The emitted photons are detected in a conjugate basis to the basis the atom has been projected on. For this analysis basis, a completely random measurement outcome is expected, i.e. a dark state population of 0.5. Therefore, these states are especially sensitive to polarisation errors. When using an atomic analysis angle of 45°, a difference of the dark state population for photon analysis in H and V indicates that there are still polarisation errors. The polarisation is adjusted by tilting the wave plate minimising the dark state population difference in H and V.

Picture 3.3 shows the projection on the dark state varying the power of the STIRAP lasers. This is done by varying the voltage applied to the AOM. (A, B): after having compensated the polarisation behind the vacuum glass cell and (C, D): after optimisation at the position of the atom. A and C are measured with STIRAP vertically polarized and B, D with a STIRAP polarisation of 45°.
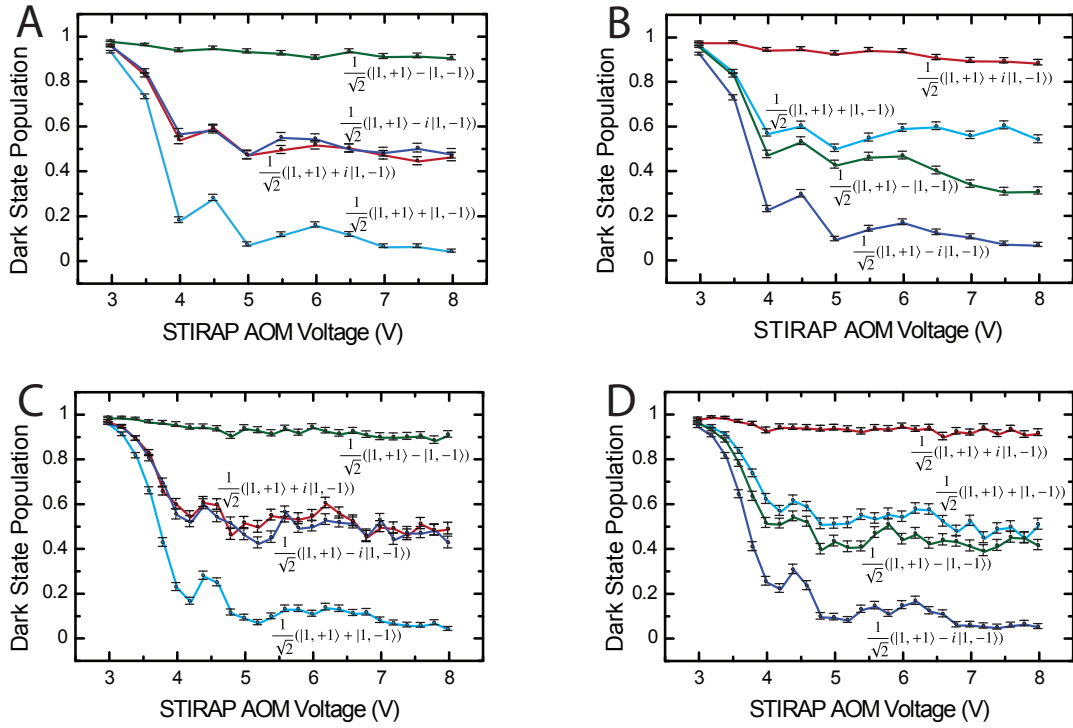
Figure 3.3: Projection on the dark state varying the power of the STIRAP lasers after pre-compensation (A, B) and after final compensation (C, D) of the polarisation. Atomic analysis in V (A, C) and 45° (B, D). One pair of the photo diodes analysis in H/V and the other one in ±45°.

3.3 Long-term Mechanical Stability of the Optical Fibre Connection

In order to entangle two remote atoms, a Bell-state-measurement has to be performed. For this purpose, the emitted photons of atom 2 need to be guided to setup 1, where the two photons of the different setups interfere. Since the polarisation degree of freedom is used to entangle the photon with the atom, it is essential that the fibre does not change the polarisation. In usual fibres, this is not the case as the polarisation changes with temperature and mechanical stress due to locally induced birefringence [35]. Polarisation-maintaining fibres are no option either as they only preserve two orthogonal linear polarisations.

In the short fibre leading to the Bell-state-measurement setup at trap 1 (5 m), polarisation changes are compensated manually by twisting the fibre. Once compensated, the polarisation is stable for days due to mechanical stability of the fibre and little thermal fluctuations. The long fibre connecting the two setups (30 m) is less stable due to its length, less mechanical stability and more exposure to thermal changes. To maintain the polarisation here, an automatic polarisation control is used which corrects for polarisation changes typically every couple of minutes during measurements [36].

3.3.1 Working Principle of the Polarisation Control

In order to correct for polarisation changes in the fibre, reference light in two non-orthogonal polarisations is sent through the fibre and detected by photo diodes. As the reference light has the same wavelength as the spontaneously emitted photons and takes the same path from the vacuum glass cell on, this allows to measure the effects of the fibre on the polarisation of the photons.

Behind the long fibre, there is a rotatable mirror whose position determines whether the transmitted light is guided to the APSs or to a polarimeter. The polarimeter (see fig. 3.4) consists of six photo diodes which allows to completely determine the polarisation of the reference light. The error of the arriving reference light to the set value is determined and a dynamic polarisation controller corrects for the error (see [32]).
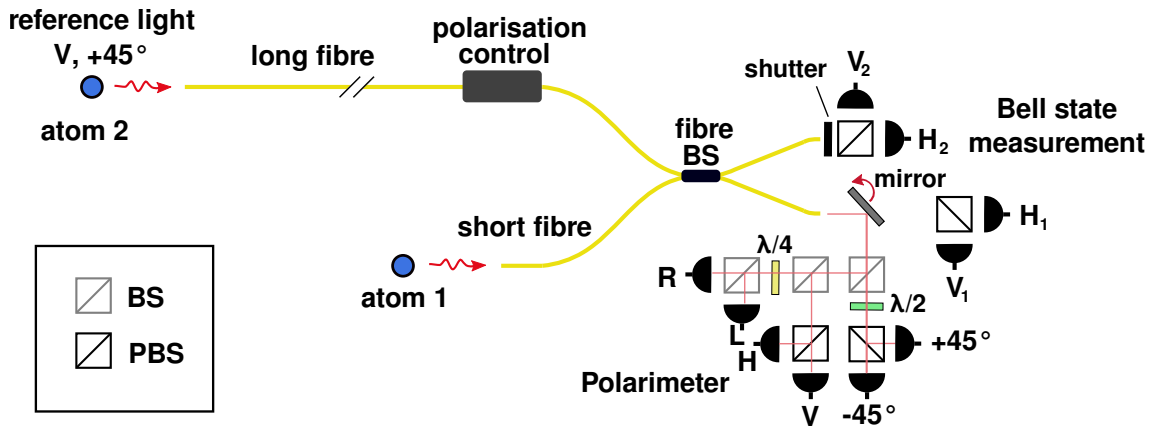
Figure 3.4: Principle of polarisation stabilisation in the long fibre: Reference light is guided through the same fibre as the emitted photons. A rotatable mirror can be placed in the beam in a way that the light goes to the polarimeter instead of being guided to the APSs.

3.3.2 Mechanical Stability of the Coupling of the Reference Light

When performing measurements which included employing the polarisation control of the long fibre, the main problem turned out to be the mechanical stability of the coupling of the reference light into the long fibre. The reference light has a long free space path before it is coupled into the fibre and its mirrors and lenses are situated on different levels. Therefore, the coupling into the long fibre was very sensitive to thermal drifts and mechanical vibrations.

Some of the mirrors of this paths had been mounted on posts of a diameter of 1/2". In order to improve mechanical stability, those 1/2" posts were replaced by more stable posts of 1" diameter. By sheltering the experiment from flows of colder or warmer air, the thermal drifts could be reduced.

Every time the polarisation compensation is run, the error as well as the sum of the voltages measured by the photo diodes are logged. The sum of the voltages is proportional to the intensity of the reference light and therewith a measure for its coupling efficiency. Picture 3.5 shows the power every time a compensation was performed. After the 12/08/2011 the connection was stable so that it run for four days without the need for manual recou-
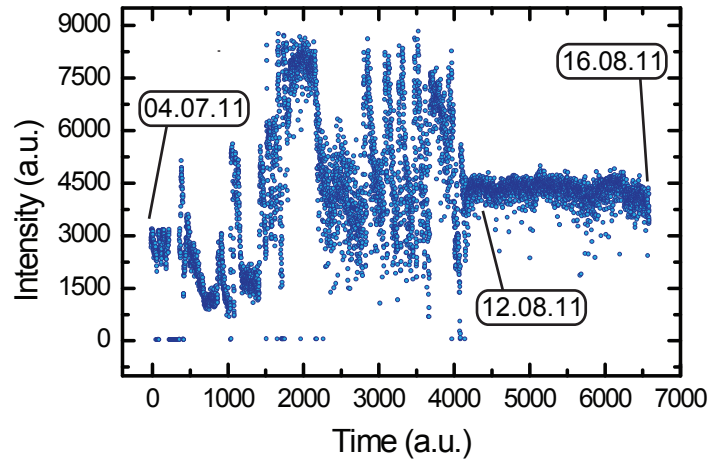
Figure 3.5: The power of the reference light which arrives at the polarimeter.

pling of the reference light.

3.4 Temporal Overlap of the Arrival Time of the Photons

An essential requirement of the two photon interference is the temporal overlap of the two arriving photons in order to perform a Bell-state measurement and carry out the entanglement swapping process.

3.4.1 Synchronization of the two Setups

The two setups are synchronized by a common clock. As soon as there is one atom in each of the traps, a start signal is distributed which makes sure that the two experiments start the excitation procedure synchronously.

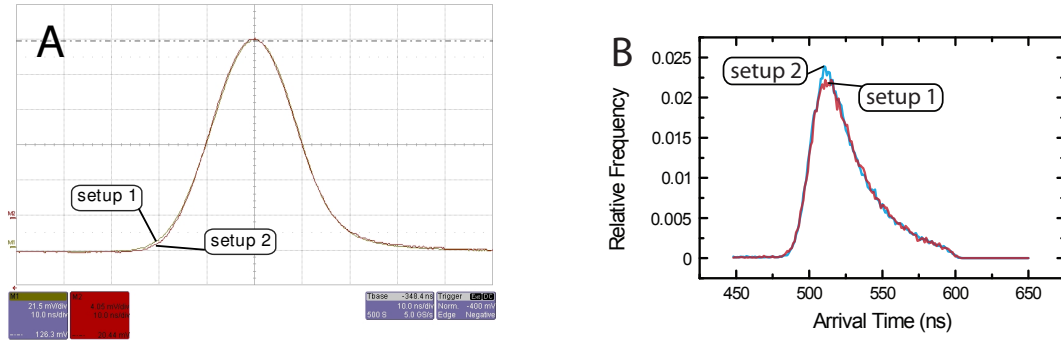Figure 3.6: A: Matching of the optical excitation pulses. B: Histogram of the arrival times of the two emitted photons at the APDs normalised to the total number of detected photons.

3.4.2 Temporal Matching of the two Emitted Photons

The temporal overlap of the emitted photons can be measured by taking a histogram of the arrival times of the photons at the APDs. In these histograms, both the shapes and the timing has to be matched. The excitation pulse is chosen to drive less than half a Rabi cycle in order to prevent the emission of two photons. At the beginning, the atom is coherently excited which determines the raising rate of the relative frequency. Because of the spontaneous emission, the population of the excited state then decays exponentially. In order to match the relative frequencies, one has to match the shapes of the excitation pulses as well as their effective Rabi frequencies (see fig. 3.6, A). In a second step a histogram of the arrival times of the photon at the APDs is recroded and the timing of the excitation pulses is changed according to the result. The two matched histograms can be seen in fig. 3.6, B.

Once a timing for the excitation pulses has been chosen, the displacement of the excitation pulse at atom 2 varies no more than 0.5 ns over several weeks.

3.5 Conclusion

The aim of the described calibration measurements was to increase the visibility of the atom-photon entanglement in setup 2 as well as its mechanical stability and the synchronization of the two setups. The improvement of the mechanical stability of the coupling of the reference light allows to operate the two setups using automatic polarisation control without the need of recoupling for several days. Picture 3.7 shows a measurement of the atom-photon entanglement in trap 2. A visibility above 90 % could be achieved. Together with the overlap of the spontaneously emitted photons, this allows to violate Bell's inequality with two entangled atoms.

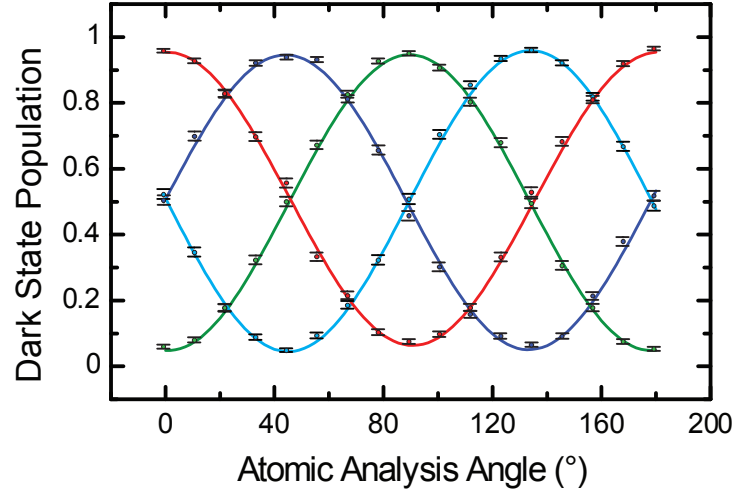
Figure 3.7: Correlations between the polarisation of the photon and the spin state of the atom. The four curves represent the projection on the dark state in the four photon analysis bases $\frac{1}{\sqrt{2}}(|1,+1\rangle + |1,-1\rangle)$, $\frac{1}{\sqrt{2}}(|1,+1\rangle - |1,-1\rangle)$ and $\frac{1}{\sqrt{2}}(|1,+1\rangle + i|1,-1\rangle)$, $\frac{1}{\sqrt{2}}(|1,+1\rangle - i|1,-1\rangle)$

4 Spin-State-Selective Ionisation

For a fast state read-out of the atom, a fast, spin-state-selective ionisation scheme is necessary which detects any desired qubit, encoded in the Zeeman-state levels, with a high fidelity. At the beginning of this chapter a brief introduction to photo ionisation of atoms is given. Then follows an explanation of the STIRAP scheme, which has been used for the spin-state detection of single ^{87}Rb atoms. A new scheme is presented and calculations are carried out to determine the expected visibility and time needed for the ionisation.

4.1 Brief Introduction to Photo Ionisation

Photo ionisation is a process in which an atom absorbs one or several photons whose total energy lies above the binding energy of an electron. Subsequently the electron is released and a positively charged ion is left behind. Here, one-photon photo ionisation is considered and the outer electron, which has the lowest binding energy, is released.

In perturbation theory, such a system can be described by a Hamiltonian of the unperturbed system plus a small interaction Hamiltonian of the atom with the light: $\mathcal{H} = \mathcal{H}_0 + \mathcal{H}_{int}$. In the framework of this theory, the rate at which the ionisation process between the initial state $|i\rangle$ and final state $|f\rangle$ happens, Γ_{if}, is given by Fermi's Golden rule [37]:

$$\Gamma_{if} = \frac{2\pi}{\hbar} |\langle f| \mathcal{H}_{int} |i\rangle|^2 \rho(E_f) \qquad (4.1)$$

where $\rho(E_f)$ is the density of states in the phase space at the energy of the final state $E_f = E_\gamma - E_{ion}$, E_γ and E_{ion} being the photon's energy and the ionisation-energy, respectively. The final states form a continuum of states, but due to the conservation of angular momentum, the ionisation cross section is state dependent [38]. The ionisation rate Γ_{if} can

also be written as a product of the ionisation cross section and the photon flux density:

$$\Gamma_{if}(\omega_\gamma, I_\gamma) = \sigma_\gamma(\omega_\gamma)\Phi \qquad (4.2)$$

where $\Phi = \frac{I_\gamma}{\hbar\omega_\gamma}$ is the photon flux density which determines the number of photons per time per area with I_γ being the intensity of the ionisation light.

Substituting Φ in 4.2, the ionisation rate can be written as:

$$\Gamma_{if}(\omega_\gamma, I_\gamma) = \frac{\sigma_\gamma(\omega_\gamma)}{\hbar\omega_\gamma}I_\gamma \qquad (4.3)$$

This means, the ionisation rate depends linearly on the intensity.

In our experiment, an ionisation laser at 450 nm is used. Its waist focused on the ^{87}Rb atom within the atomic trap is 1.13 μm. Assuming a cross section of $\sigma = 12.24 \cdot 10^{-22}$ m^2 for an ionisation from the 5^2P state (which is the average of the measured cross sections shown in fig. 4.1), the ionisation rate depends on the power P of the ionisation laser as follows:

$$\Gamma_{if}(\omega_\gamma, I_\gamma) = \frac{\sigma}{\hbar\omega_\gamma}\frac{2P}{\pi w_0} = 1.0438 \cdot 10^9 \frac{1}{Ws} P \qquad (4.4)$$

To achieve, for instance, an ionisation rate which is equal to the spontaneous decay rate of $\frac{1}{26\,ns}$, a power of 37 mW is necessary.

Theoretical calculations by Aymar et al. [39] of the wavelength dependency of the ionisation of the 5^2P state of ^{87}Rb predict a maximal cross section at the ionisation threshold ($\lambda_{thr} = 473.7$ nm from $5^2P_{1/2}$ and $\lambda_{thr} = 479.1$ nm from $5^2P_{3/2}$), decaying monotonously when increasing the energy of the photons used for ionisation. This happens on an energy scale of electron volts. As one electron volt corresponds to 1240 nm, no change of the cross section on the scale of nanometers is expected.

There have been several measurements of the ionisation cross section of the $5^2P_{3/2}$ state of ^{87}Rb at different wavelengths, see fig. 4.1. No decrease of the ionisation cross section between 476.5 nm and 407 nm can be observed in experiments. Therefore, a wide range of wavelengths can be used for our experiment.
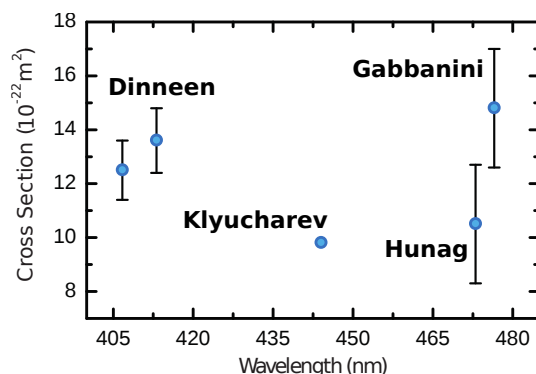
Figure 4.1: Measured ionisation cross section of the $5^2 P_{3/2}$ state of ^{87}Rb for different wave lengths [40, 41, 42]

4.2 Master Equation for the Description of Spontaneous Emission and Ionisation

In our model (see 4.5.1), the ionisation is considered mathematically as spontaneous decay. In order to describe spontaneous optical emission in the dipole approximation, one has to consider the interaction of the atom with the vacuum. Consider a two level system with the states $|g\rangle$ and $|e\rangle$, together with the Schrödinger equation for the density matrix in the interaction picture [43]:

$$\hbar \frac{\partial}{\partial t}\hat{\rho}(t) = -\frac{i}{\hbar}[V_{vac}(t), \hat{\rho}(t)] \tag{4.5}$$

with $\hat{\rho}(t) = \hat{\rho}_A(t) \otimes \hat{\rho}_V(t)$ where $\hat{\rho}_A(t)$ describes the atom and $\hat{\rho}_V(t)$ the vacuum and $V_{vac}(t)$ being the interaction Hamiltonian which describes the interaction of an atom with the vacuum.

By defining:

$$\vec{d}_{ij} = e \langle i | \vec{r} | j \rangle$$

$$A_{ij} = |i\rangle \langle j|$$

$$g_{\vec{k}}^{ij} = \frac{(\vec{d}_{ij}\hat{e}_{\vec{k}})\epsilon_k}{\hbar}$$

where: $\hat{e}_{\vec{k}}$ is the polarisation vector, $\epsilon_k = \sqrt{\frac{\hbar\nu_{veck}}{2\epsilon_0 V}}$, V the quantisation volume and $\nu_{\vec{k}}$ the frequency of the lightfield with wave vector $\vec{k}$

and the matrices:

$$\sigma_z = A_{ee} - A_{gg} \tag{4.6}$$

$$\sigma_+ = A_{eg} \tag{4.7}$$

$$\sigma_- = A_{ge}, \tag{4.8}$$

the Hamiltonian in the interaction picture with a quantised electrical field is given by:

$$V = \hbar \sum_{\vec{k}} (g_{\vec{k}}\sigma_+ a_{\vec{k}} e^{i(\omega-\nu_{\vec{k}})} + g_{\vec{k}}^*\sigma_- a_{\vec{k}}^+ e^{-i(\omega-\nu_{\vec{k}})}) \tag{4.9}$$

where ω is the atomic transition frequency.

After several approximations which assume a weak coupling and no memory of the vacuum, and after tracing over the vacuum and applying the Wigner-Weisskopf approximation, the Master Equation for spontaneous emission is obtained:

$$\frac{d}{dt}\rho_A(t) = -\frac{\Gamma}{2}(\sigma_+\sigma_-\rho_A(t) + \rho_A(t)\sigma_+\sigma_- - 2\sigma_-\rho_A(t)\sigma_+) \tag{4.10}$$

where Γ is the spontaneous emission rate. Adding this to the Schrödinger equation , the dynamics of a two level system including spontaneous emission is described by:

$$\frac{d}{dt}\rho_A(t) = -\frac{i}{\hbar}[V, \rho_A(t)] - \frac{\Gamma}{2}(\sigma_+\sigma_-\rho_A(t) + \rho_A(t)\sigma_+\sigma_- - 2\sigma_-\rho_A(t)\sigma_+) \tag{4.11}$$

The ionisation process is in principle a coherent process to a defined state. This state,

however, has a very fast decay channel to the state in which the electron is separated from the ion which is not reversible. If the separation of the electron from the ion happens considerably faster than the one Rabi period of the ionisation laser (which is the case for all parameters used in this work), the intermediate state can be neglected and the ionisation process can be treated like a spontaneous decay.

4.3 Ionisation Scheme using STIRAP

4.3.1 Theoretical description of the STIRAP Process

The STIRAP [28] process allows to coherently transfer a population from the state $|1\rangle$ to the state $|2\rangle$ mediated by a state $|e\rangle$ with the transitions $|1\rangle \rightarrow |e\rangle$ and $|2\rangle \rightarrow |e\rangle$ being optically allowed. The lasers driving these transitions have the Rabi frequencies Ω_1 and Ω_2. To describe this system mathematically, consider a Λ-System with the states: $|1\rangle$, $|2\rangle$ and $|e\rangle$ (see fig. 4.2). In order to use matrix notation, we define:

$$|e\rangle \widehat{=} \begin{pmatrix} 1 \\ 0 \\ 0 \end{pmatrix}, \qquad |1\rangle \widehat{=} \begin{pmatrix} 0 \\ 1 \\ 0 \end{pmatrix}, \qquad |2\rangle \widehat{=} \begin{pmatrix} 0 \\ 0 \\ 1 \end{pmatrix}$$

With the two Rabi frequencies Ω_1, and Ω_2 (see fig. 4.2) at resonance, the Hamiltonian in the interaction picture is given by:

$$V = \hbar \begin{pmatrix} 0 & \Omega_1 & \Omega_2 \\ \Omega_1 & 0 & 0 \\ \Omega_2 & 0 & 0 \end{pmatrix} \tag{4.12}$$
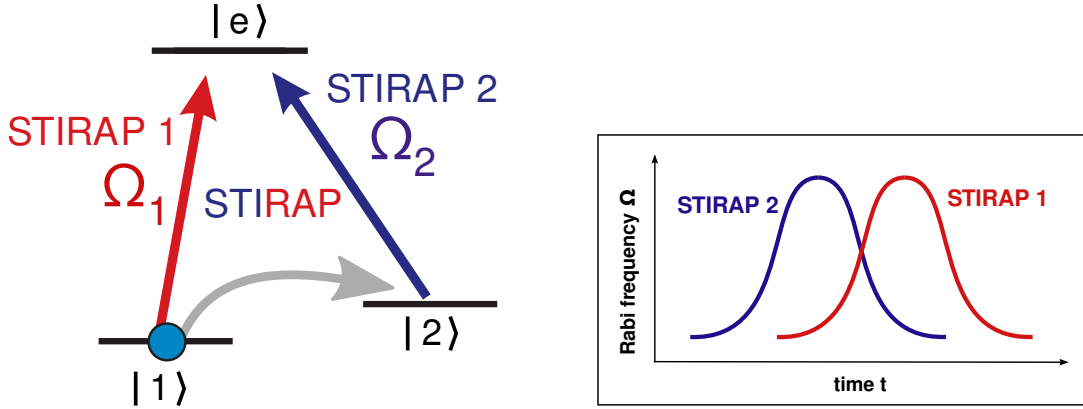
Figure 4.2: Scheme of the STIRAP process. (left): Levels and lasers involved in a STIRAP transfer, (right): Pulse sequence used for STIRAP

The eigenstates and their respective eigenvalues are:

$$|\Psi_D\rangle = \frac{1}{\sqrt{|\Omega_1|^2 + |\Omega_2|^2}} \begin{pmatrix} 0 \\ \Omega_2 \\ \Omega_1 \end{pmatrix} \qquad \text{with } \lambda_D = 0,$$

$$|+\rangle = \frac{1}{\sqrt{2}} \frac{1}{\sqrt{|\Omega_1|^2 + |\Omega_2|^2}} \begin{pmatrix} \sqrt{|\Omega_1|^2 + |\Omega_2|^2} \\ \Omega_2 \\ \Omega_2 \end{pmatrix} \quad \text{with } \lambda_+ = \frac{\hbar}{2} \sqrt{|\Omega_1|^2 + |\Omega_2|^2}, \qquad (4.13)$$

$$|-\rangle = \frac{1}{\sqrt{2}} \frac{1}{\sqrt{|\Omega_1|^2 + |\Omega_2|^2}} \begin{pmatrix} -\sqrt{|\Omega_1|^2 + |\Omega_2|^2} \\ \Omega_1 \\ \Omega_2 \end{pmatrix} \quad \text{with } \lambda_- = -\frac{\hbar}{2} \sqrt{|\Omega_1|^2 + |\Omega_2|^2}$$

The light field does not couple to $|\Psi_D\rangle$ as:

$$V|\Psi_D\rangle = \frac{1}{\sqrt{|\Omega_1|^2 + |\Omega_2|^2}} (\Omega_1\Omega_2 |e\rangle - \Omega_2\Omega_1 |e\rangle) = 0 \qquad (4.14)$$

This means, STIRAP 1, and STIRAP 2 interfere destructively and therefore do not couple $|\Psi_D\rangle$ to $|e\rangle$.

For the STIRAP scheme, let's start with the atom in state $|1\rangle$. The laser pulses which are then applied to the atom are shown in fig. 4.2. When the change of the Hamiltonian (i.e. the change of Ω_1 and Ω_2) occurs adiabatically, the atom stays in its eigenstate. Now, the state of the atom is considered at three different times:

1. $\Omega_1 = 0$, Ω_2 **weak**

   As Ω_2 does not couple to $|1\rangle$, the atom is in $|\Psi_D\rangle = |1\rangle$

2. Ω_1, Ω_2 **on**

   For (almost) arbitrary Ω_1, Ω_2: $V|\Psi_D\rangle = 0$, the light does not couple to $|\Psi_D\rangle$ and the atom remains in its eigenstate.

3. $\Omega_2 = 0$, Ω_1 **weak**

   Since the atom is still in the same eigenstate, it has to be in state $|\Psi_D\rangle = |2\rangle$

This means, the atom stays in the eigenstate $|\Psi_D\rangle$ during the whole process while the eigenstate is adiabatically changed and the atom is therefore transferred from $|1\rangle$ to $|2\rangle$. Ideally, the transfer probability approaches unity and since there is no spontaneous emission involved, the process is quite robust.

4.3.2 Application of the STIRAP Process in our Experiment

The STIRAP process is used in our experiment for the spin-state detection (see fig. 4.3, A) to transfer the atom from the $5^2S_{1/2}$, $F = 1$ state to the $5^2S_{1/2}$, $F = 2$ with an additional feature: Only a chosen superposition of $|1, \pm1\rangle$ is transferred [29]. This spin-selectivity is based on selection rules for optical transitions: Every polarisation of the STIRAP 1 can be written as a superposition of σ^+ and σ^- light. Therefore, considering the interaction Hamiltonian when only Ω_1 is turned on, for every polarisation of STIRAP 1, there is a bright state which couples to Ω_1 and an orthogonal dark state which does not. Consequently, only the bright state is transferred to $F = 2$ in the STIRAP process.

Once the chosen superposition has been transferred to $F = 2$ the atom can be ionised by a two step ionisation via the excited state $5^2P_{3/2}$, $F' = 3$ using the cycling and the ionisation laser.
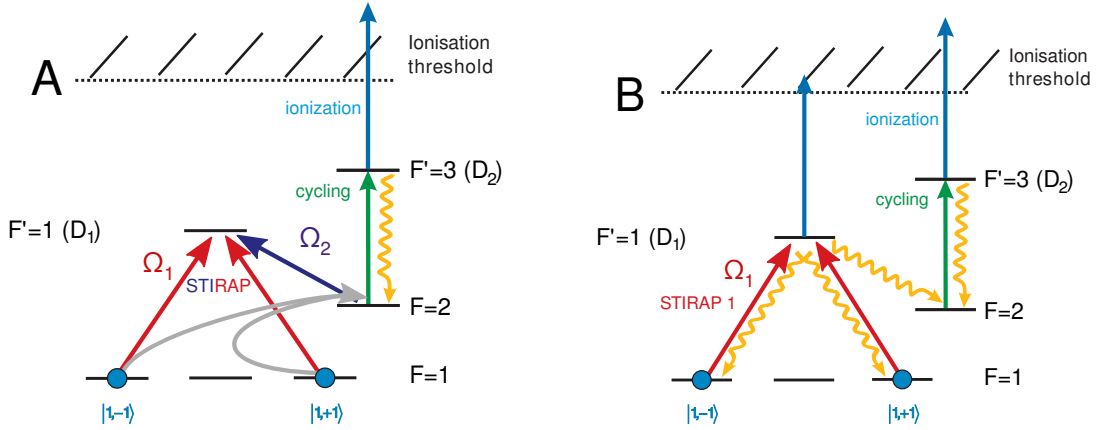
Figure 4.3: A: Scheme for spin-state detection using STIRAP. B: Scheme for spin-state detection by direct ionisation.

Time needed for the Ionisation

The time which is needed to ionise the atom consists of two parts: the time one needs to transfer the atom to the $F = 2$ state (120 ns [22]) and the time needed for the two step ionisation. The ionisation time constant achieved so far is 21.1 (+1.1-2.7) ns (see chapter 6), which means that it takes 92 ns to ionise the atom with a probability of 98.7 % (which corresponds to a fidelity of 99 %). This means, to achieve a fidelity of over 99 %, a total detection time of 120 ns + 92 ns = 212 ns is necessary.

4.4 Scheme for Direct Ionisation

A spin-state detection scheme which does not require a STIRAP transition is potentially simpler and faster. It requires sufficient power of the ionisation laser such that the ionisation time is shorter than the natural lifetime of the excited state ($5^2P_{1/2}$), because spontaneous optical decay and ionisation are the two competing processes once the atom has been excited. The scheme is shown in fig. 4.3, B. The former STIRAP 1 laser will from now on be referred to as Ω_1 in order to avoid confusion as it is no longer used for a STIRAP transfer. It excites a chosen superposition of $|1, \pm 1\rangle$ to the $5^2P_{1/2}$, $F' = 1$ state, from where the atom can be ionised, but it also decays with a certain probability by spontaneous emission. If this happens, the atom decays with the probability of 5/6 into the

$5^2S_{1/2}$, $F = 2$ state, and with a probability of 1/12 in the dark and the bright state each. These relative transition ratios are determined by the Clebsch-Gordan coefficients [44]. If the atom decays to the $5^2S_{1/2}$, $F = 2$ state, it can be ionised like in the previously discussed scheme using the cycling and the ionisation laser. If the atom decays into the bright state, it can be excited again by Ω_1, but, if the atom ends up in the dark state, it cannot be ionised any more and this leads to errors in the spin-state read-out.

4.5 Computation of the Scheme of Direct Ionisation

In this section a model is presented which allows to calculate the dynamics of the six level system involved in the process of direct ionisation (see fig. 4.4). Using this model, one can estimate the time needed for the complete ionisation process and the achievable fidelity of the atomic state detection.
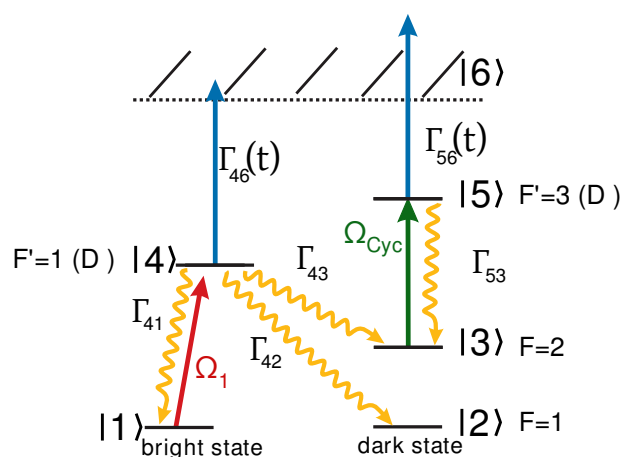

Figure 4.4: Six level model used for the calculations

4.5.1 The Model used for Computation

As the ionisation cross section is difficult to calculate, this model is limited to treat the ionisation similar to a spontaneous emission process with the "decay rate" Γ_{ion} which has to be determined experimentally. As laser pulses are used, a time dependent Rabi

frequency $\Omega(t)$ and ionisation rate $\Gamma_{ion}(t)$ are considered which vary with the shape of the optical laser pulses $f(t)$:

$$\Omega(t) = \Omega_0 \cdot \sqrt{f_1(t)} \qquad \text{and} \qquad \Gamma_{ion}(t) = \Gamma_{ion} \cdot f_{ion}(t) \qquad (4.15)$$

The laser pules of the cycling laser and Ω_1 are approximated by a rising Gaussian edge, a plateau and a falling Gaussian edge. The ionisation laser has very steep edges so that no rising/ falling time is considered. The lasers Ω_1 and cycling, which are resonant to their respective transitions, are considered together with all possible decays (see fig. 4.4). The ionisation is also treated as spontaneous decay.

4.5.2 Calculation

The Master equation for a two level system with the levels $|g\rangle$ $|e\rangle$ reads (see Eq 4.11):

$$\frac{d}{dt}\rho(t) = -\frac{i}{\hbar}[V,\rho] - \frac{\Gamma}{2}(\sigma_+\sigma_-\rho(t) + \rho(t)\sigma_+\sigma_- - 2\sigma_-\rho(t)\sigma_+) \qquad (4.16)$$

This can be generalized to a six level system:

$$\frac{d}{dt}\rho(t) = -\frac{i}{\hbar}[V,\rho] - \underbrace{\sum_{i,j}\frac{\Gamma_{ij}}{2}(A_{ji}A_{ij}\rho(t) + \rho(t)A_{ji}A_{ij} - 2A_{ij}\rho(t)A_{ji})}_{D} \qquad (4.17)$$

Γ_{ij} is the spontaneous emission rate from the state $|i\rangle$ to $|j\rangle$ and is zero if there is no spontaneous emission between these two levels.

In the interaction picture, the interaction Hamiltonian for our system is:

$$V = \begin{pmatrix} 0 & 0 & 0 & \Omega_{STR}(t) & 0 & 0 \\ 0 & 0 & 0 & 0 & 0 & 0 \\ 0 & 0 & 0 & 0 & \Omega_{Cyc}(t) & 0 \\ \Omega_{STR}(t) & 0 & 0 & 0 & 0 & 0 \\ 0 & 0 & \Omega_{Cyc}(t) & 0 & 0 & 0 \\ 0 & 0 & 0 & 0 & 0 & 0 \end{pmatrix} \qquad (4.18)$$

The dissipation part of the equation looks as follows:

$$D = \begin{pmatrix} d_{11} & d_{12} & d_{13} & d_{14} & d_{15} & d_{16} \\ d_{21} & d_{22} & d_{32} & d_{24} & d_{25} & d_{26} \\ d_{31} & d_{32} & d_{33} & d_{34} & d_{35} & d_{36} \\ d_{41} & d_{42} & d_{43} & d_{44} & d_{45} & d_{46} \\ d_{51} & d_{52} & d_{53} & d_{54} & d_{55} & d_{56} \\ d_{61} & d_{62} & d_{63} & d_{64} & d_{65} & d_{66} \end{pmatrix} \tag{4.19}$$

where the components are:

$$d_{11} = \Gamma_{41}\rho_{44}$$

$$d_{22} = \Gamma_{42}\rho_{44}$$

$$d_{33} = \Gamma_{43}\rho_{44} + \Gamma_{53}\rho_{55}$$

$$d_{44} = -(\Gamma_{41} + \Gamma_{42} + \Gamma_{43} + \Gamma_{46})\rho_{44}$$

$$d_{55} = -(\Gamma_{53} + \Gamma_{56})\rho_{55}$$

$$d_{66} = \Gamma_{46}\rho_{44} + \Gamma_{56}\rho_{55}$$

$$d_{14} = d_{41} = -\frac{1}{2}(\Gamma_{41} + \Gamma_{42} + \Gamma_{43} + \Gamma_{46})\rho_{14}$$

$$d_{15} = d_{51} = -\frac{1}{2}(\Gamma_{53} + \Gamma_{56})\rho_{15}$$

$$d_{24} = d_{42} = -\frac{1}{2}(\Gamma_{41} + \Gamma_{42} + \Gamma_{43} + \Gamma_{46})\rho_{24} \tag{4.20}$$

$$d_{25} = d_{52} = -\frac{1}{2}(\Gamma_{53} + \Gamma_{56})\rho_{25}$$

$$d_{34} = d_{43} = -\frac{1}{2}(\Gamma_{41} + \Gamma_{42} + \Gamma_{43} + \Gamma_{46})\rho_{34}$$

$$d_{35} = d_{53} = -\frac{1}{2}(\Gamma_{53} + \Gamma_{56})\rho_{35}$$

$$d_{45} = d_{54} = -\frac{1}{2}(\Gamma_{41} + \Gamma_{42} + \Gamma_{43} + \Gamma_{46} + \Gamma_{53} + \Gamma_{56})\rho_{45}$$

$$d_{46} = d_{64} = -\frac{1}{2}(\Gamma_{41} + \Gamma_{42} + \Gamma_{43} + \Gamma_{46})\rho_{46}$$

$$d_{56} = d_{65} = -\frac{1}{2}(\Gamma_{53} + \Gamma_{56})\rho_{56}$$

$$d_{12} = d_{21} = d_{13} = d_{31} = d_{16} = d_{61} = d_{23} = d_{32} = d_{26} = d_{62} = d_{36} = d_{63} = 0$$

In total, there are 36 differential equations for $\rho(t)$ which were numerically solved using Mathematica.

Parameters

The Rabi frequencies can be calculated by [1]:

$$\Omega = \Gamma \sqrt{\frac{I}{2I_{sat}}} \tag{4.21}$$

where Γ is the natural linewidth, I the intensity of the laser at the atom and I_{sat} the saturation intensity of the transition.

The intensity of a Gaussian beam is calculated using the waist w_0 and the Power P [50]:

$$I = \frac{2P}{\pi w_0^2} \tag{4.22}$$

The following parameters are used for the calculations:

$$I_{Cyc} = 335 \cdot I_{sat,Cyc}$$

$$\Gamma_0 = 2\pi \, 5.746 \cdot 10^6 \, \frac{1}{s} \text{ total decay rate } D_1$$

$$\Gamma_{41} = \frac{1}{12}\Gamma_0$$

$$\Gamma_{42} = \frac{1}{12}\Gamma_0$$

$$\Gamma_{43} = \frac{5}{6}\Gamma_0$$

$$\Gamma_{53} = 1.0555 \cdot \Gamma_0 \text{ total decay rate } D_2$$

The intensity of Ω_1, the "decay rates" for the ionisation Γ_{46} and Γ_{56}, as well as the length of the pulses are varied.

4.5.3 Results

In order to give an overview of the evolution of the considered system, different parameter settings have been chosen.
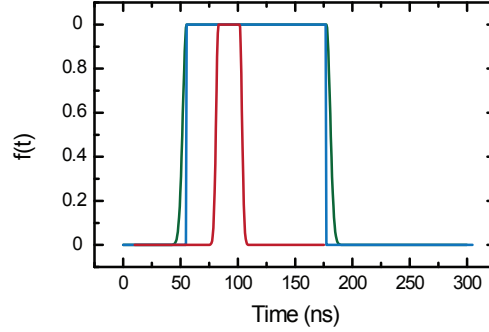
Figure 4.5: Pulse sequence used for the calculations. Blue: ionisation, red: Ω_1, green: cycling.

In a first calculation, the optical pulses are chosen as shown in fig. 4.5. The Ω_1-pulse is chosen to be 24 ns as such pulses can still be generated by our AOMs.

Dependence of the Ionisation Probability on the Ionisation Rate

We set $\Gamma_{ion} = \Gamma_{46} = \Gamma_{56} = 2 \cdot \Gamma_0$, and choose Ω_1 such that the excitation to F = 1 is maximized, i.e. Ω_1 drives half a Rabi cycle and no coherent depopulation takes place.

The results of the calculations of the different populations as a function of the ionisation rate Γ_{ion} are shown in fig. 4.6, where ρ_{66} is the ionisation probability, ρ_{22} the population of the dark state and ρ_{11} the population of the bright state. The first guess would be that the ionisation probability increases when increasing the ionisation rate. However, a maximum at $\Gamma_{ion} \approx 2.5 \cdot \Gamma_0$ shows, that a different effect has to be considered: With an increasing ionisation rate, the excitation also has to occur faster in order to reach a maximum of the population of the excited state at all (which in our case also means a maximum of the ionisation probability).
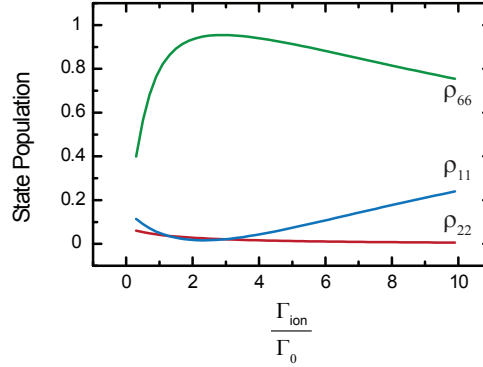
Figure 4.6: Population of ρ_{66}, ρ_{22} and ρ_{11} as function of Γ_{ion} for a P(Ω_1) chosen such that the excitation is maximised for $\Gamma_{ion} = 2\Gamma_0$

Dependence on the Ionisation Rate

In order to calculate the maximal ionisation probability for different ionisation rates, the ionisation rate $\Gamma_{ion} = \Gamma_{46} = \Gamma_{56}$ is varied in multiples of Γ_0 while the intensity of Ω_1 is adjusted such that the excitation is maximised. The intensities of Ω_1 needed are summarised in table 4.1.

Γ_{ion} (Γ_0)	1	1.5	2	2.5	3	4	5
I_{Ω_1} (I_{Sat})	348	375	413	448	489	575	672

Table 4.1: Adjustment of I_{Ω_1} so that the excitation by Ω_1 is maximised for a pulse of 24 ns.

The results of the ionised ratio of the atoms is shown in fig. 4.8, A. To ionise more than 97.5 %, an ionisation rate of 4 times the rate of the spontaneous decay is necessary. The dynamics of all populations can be seen in fig. 4.7.

Direct Ionisation without Cycling Laser

In a spontaneous decay from $5^2P_{1/2}$, the atom decays with a probability of 1/12 into the F = 2 state of the ground state. The cycling laser in the above calculations has the task to
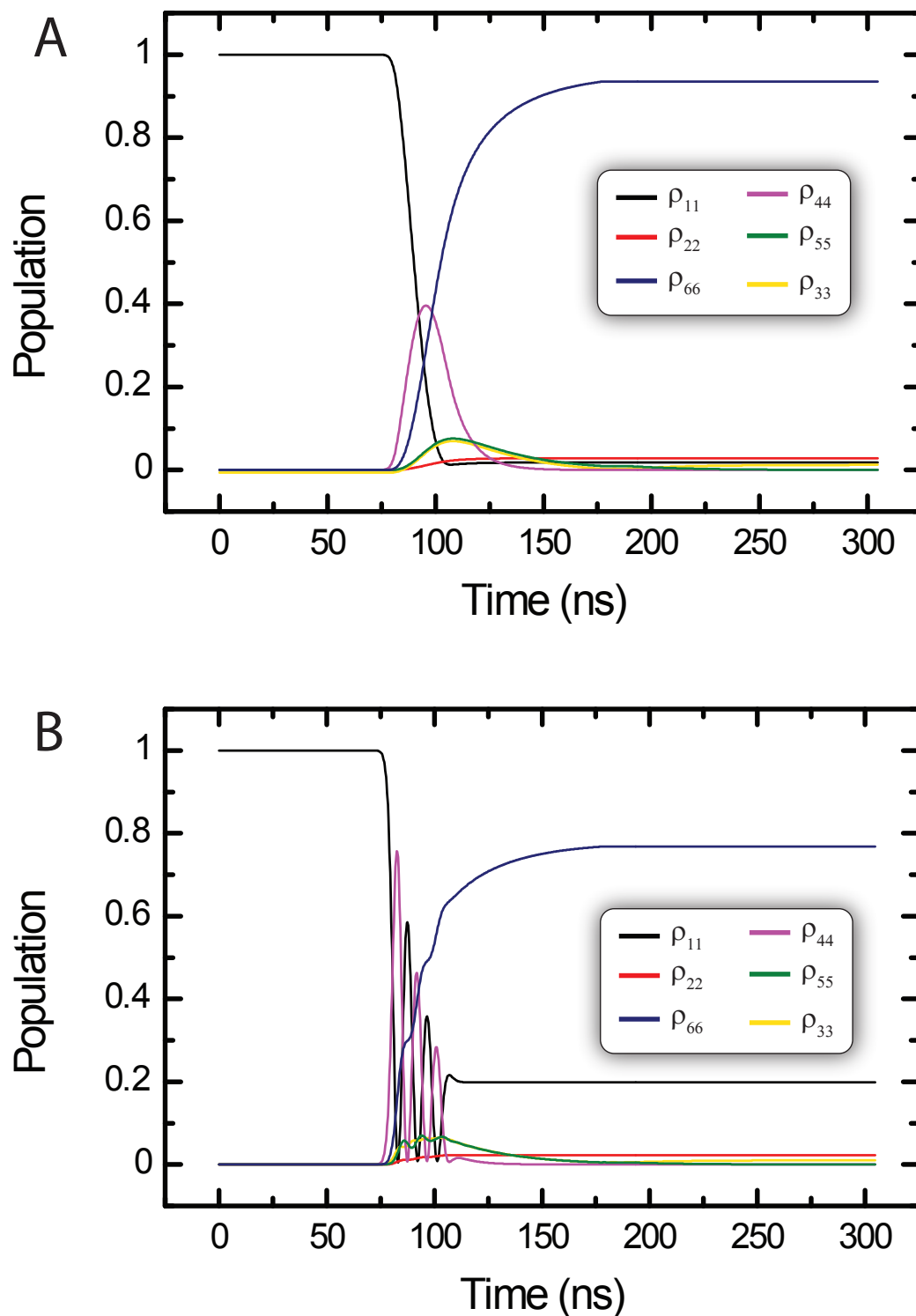
Figure 4.7: Dynamics of the populations for $\Gamma_{ion} = 2\Gamma_0$. A: half a Rabi cycle; B: more than three Rabi cycles.
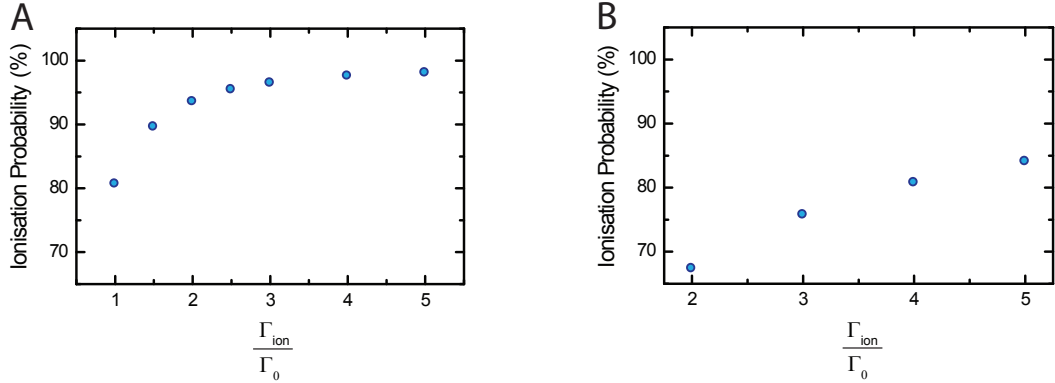
Figure 4.8: Ionisation probability versus ionisation rate when half a Rabi cycle is driven by Ω_1. A: Using cycling laser, B: Without cycling laser.

ionise the atom from the F = 2 state. A calculation of the ionisation probability without the use of the cycling laser as a function of Γ_{ion} is shown in fig. 4.8, B. It shows that with five times the power of the solid state laser system of section 5.4.1, no detection fidelity above 90 % can be achieved and the use of the cycling laser is required.

Using Longer Pulses

In the second part, we consider longer pulses. Ω_1 is turned on for 150 ns and ionisation and cycling are turned on for approx. 300 ns, starting approx. 25 ns before Ω_1 (see fig. 4.9).

The ionisation probability as well as the dark state population as a function of the ionisation rate are shown for these pulses in fig. 4.10. The power of Ω_1 is chosen to maximize the excitation at $\Gamma_{ion} = 2\Gamma_0$. This is the case for $I(\Omega_1) = 228\ I_{sat}$ (compare with 4.1). The maximum shows that also for pulses of 150 ns, it would still be necessary to adjust the power of Ω_1 for each Γ_{ion} although the effect is much smaller compared to the 24 ns pulse (compare fig. 4.6). For an ionisation laser power corresponding to $\Gamma_{ion} = 2.6\ \Gamma_0$ (see chapter 6), the atom is ionised after 300 ns with a probability of 97.7 %.
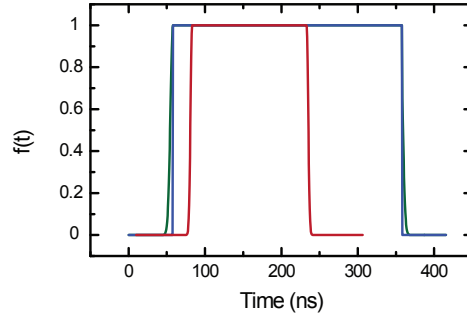
Figure 4.9: Pulse sequence used for the calculations. Blue: ionisation, red: Ω_1, green: cycling
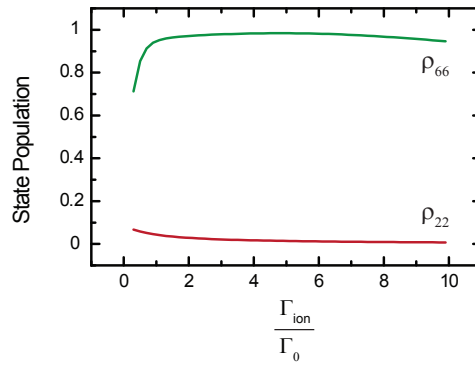

Figure 4.10: Population of ρ_{66} and ρ_{22} as function of Γ_{ion} for a I_{Ω_1} chosen such that the excitation is maximised for $\Gamma_{ion} = 2\Gamma_0$

Limitations of the Model used for the Calculations

The calculations presented here consider the ionisation probability of the state $|4\rangle$ and $|5\rangle$ to be equal, which is only an approximation. Furthermore, no detuning of the lasers is considered. This would introduce additional terms in the interaction Hamiltonian V. Furthermore, no off-resonant excitations are considered, but an analysis of the error introduced by this can be done as follows:

Errors due to Off-Resonant Scattering of the Dark State to $5^2P_{1/2}$, $F = 2$

The off-resonant excitation of the atom from the dark state to $5^2P_{1/2}$, $F = 2$ causes errors in the state detection. The scattering rate in general is given by [1]:

$$\Gamma_p = \frac{\Gamma}{2} \frac{I}{I_{sat}} \frac{1}{1 + (\frac{I}{I_{sat}}) + (\frac{2\delta}{\Gamma})^2} \tag{4.23}$$

where $\Gamma = 5.746$ MHz is the natural line width, I_{sat} the saturation Intensity and $\delta = 813$ MHz the detuning.

Inserting an intensity of $I = 228\ I_{sat}$ (which has been used in the calculations for a Ω_1-pulse of 150 ns, see fig. 4.10) yields:

$$\Gamma_p = 8097 \frac{1}{s}. \tag{4.24}$$

During a pulse of Ω_1 of 150 ns, the probability to scatter one photon is given by: $150ns \cdot 8097\frac{1}{s} = 0.001$. This means, the off-resonant scattering causes an error of 0.1 % and therefore can be neglected.

4.6 Conclusion

The two discussed schemes present methods to fast and efficiently detect the spin-state of an atom. While the STIRAP scheme works well also for smaller powers of the ionisation laser, the scheme using direct ionisation requires an ionisation rate of several times the decay rate. Its advantage is a potentially faster state read-out as no transfer to the $F = 2$ state is necessary before the ionisation can be started. The calculations show that a

visibility of over 97.7 % in 300 ns is theoretically achievable if an ionisation rate of $2.6 \cdot \Gamma_0$ can be provided. As lower intensities of Ω_1 are necessary for the new scheme, off-resonant coupling of the dark state to the F = 2 level can be neglected. For the intensities available with the new blue laser (see chapter 5), calculations predict that the STIRAP scheme works better, but this still has to be experimentally checked. For higher powers of the ionisation laser, the scheme of direct ionisation becomes faster while the STIRAP-scheme is limited due to the need of an adiabatic STIRAP transfer. Both schemes, however, are able to complete the detection within 300 ns which allows to use them for a loophole free test of Bell's inequality as in such a test, the state detection has to be completed within 1 μs, including the choice of a random measurement basis (100 ns [31, 22]) and the detection time of the ionisation fragments (< 500 ns [2]).

5 Pulsed Diode Laser Light Source for Ionisation

In order to enable fast ionisation of ^{87}Rb atoms, a laser source with $\lambda < 474$ nm and high output power is necessary. In this chapter, the setup of a pulsed diode laser of 450 nm is described and its performance is discussed.

5.1 Laser Diodes

With the development of new technologies, especially Blu Ray Disc^{TM}and new diodes for video projectors, new, more powerful blue laser diodes are designed and fabricated. The most powerful blue to ultraviolet diodes can be found at 405 nm, but there are also some available at 450 nm. As explained in section 4.1, the difference of the ionisation cross section for those two wavelengths is negligible. However, the optics of the main experiment is not designed for ultra violet light so that it is preferable to use laser diodes at around 450 nm in order to avoid major changes of the running experiment.

A transversally multi-mode[1] and a single-mode[2] diode by Nichia were tested. The main characteristics of them are summarized in table 5.1.

	NDB7352	NDB4116B
central wavelength (nm)	445	445
max. opt. output power (mW)	1000	100
transverse mode	multi-mode	single-mode
typical current (mA) at max. output	1000	100
slope efficiency (W/A)	0.8 - 1.8	0.8 - 1.8
beam divergence (°) (‖ and ⊥)	5 and 30	7 and 17

Table 5.1: Main properties of the employed Nichia diodes
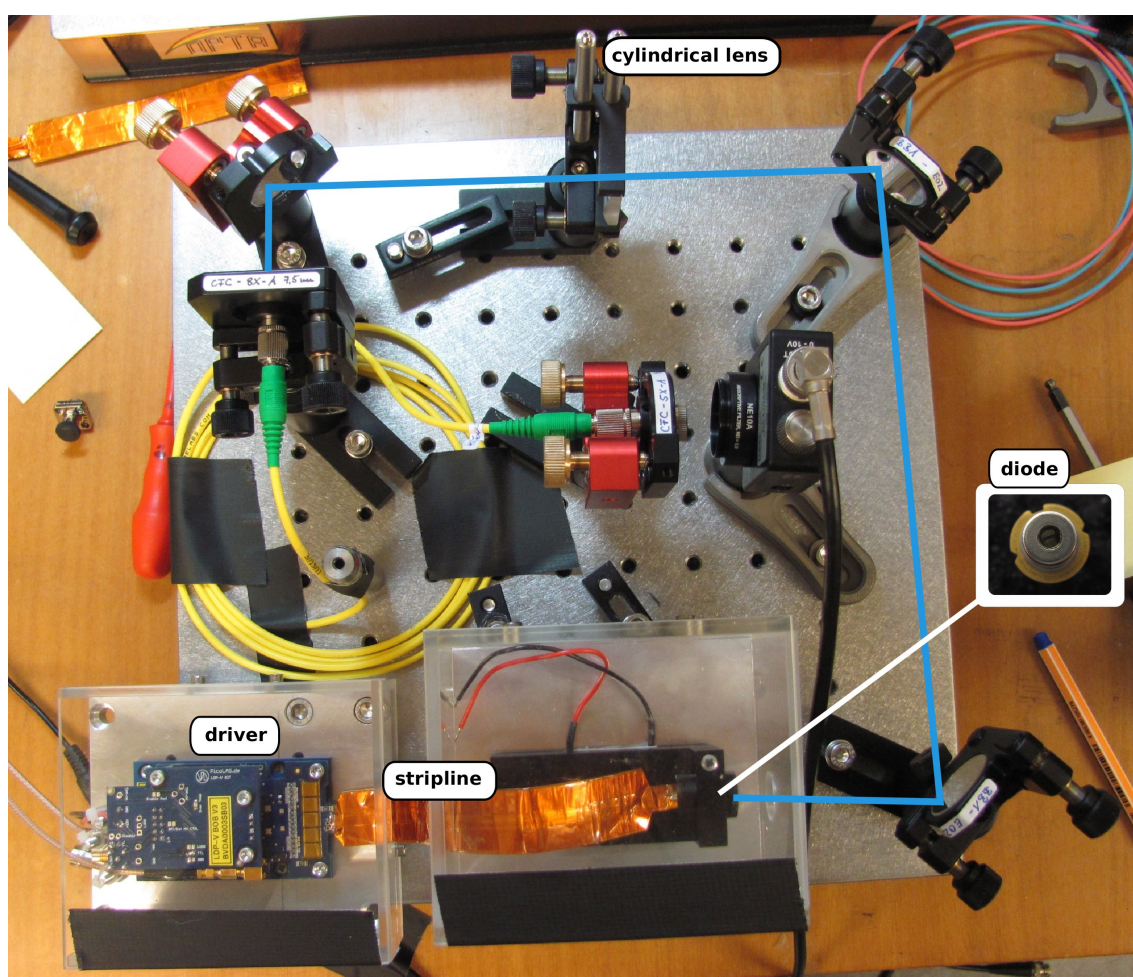

Figure 5.1: Picture of the laser setup. The coupler was later exchanged by a more stable one provided by Schäfter und Kirchhoff.

5.2 Mechanical Setup and Current Driver

The laser was set up on a 30 cm × 30 cm optical breadboard A Picture of the setup is show in fig. 5.1. The laserbox was designed such that the beam height is only 5 cm in order to avoid mechanical instabilities. The laser diode is mounted in a collimation tube together with a collimation lens. The collimation tube is held by a block of aluminium which has attached a thermistor to monitor temperature which in term is controlled by a PID controller and a peltier element. The block is put on an o-ring in order to damp vibrations [45]. A technical drawing can be seen in fig. 5.2.
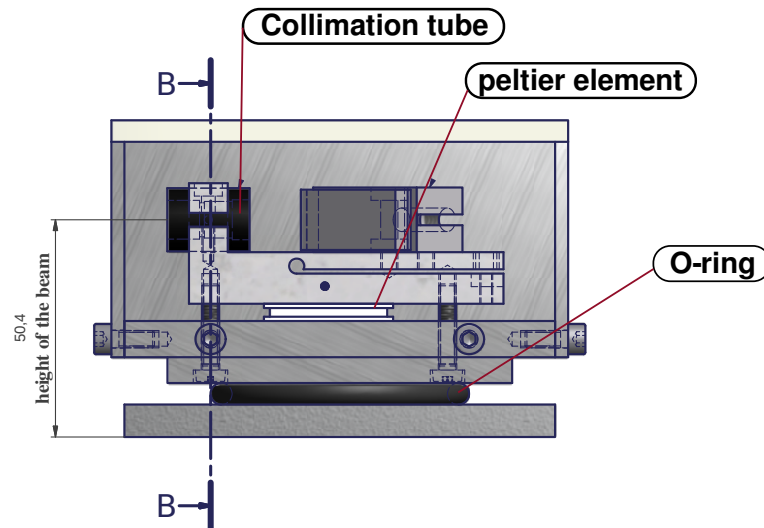

Figure 5.2: Box used for the ionisation laser. The holder for the grating seen on the picture is not necessary for this laser and therefore not implemented in our setup. With kind permission by Wolfgang Simon.

The laser diode is operated by a pulsed current driver[3] which is able to generate pulses of several hundred nanoseconds as needed for the experiment. It is specified to provide an output current of 0.3 to 3 A, a minimal pulse duration of 1 ns and a maximum rising time of 1.2 ns.

---

[1]NDB7352

[2]NDB4116B

[3]LDP-V 03-100 UF3 by Picolas together with the attachable board LDP-V BOB

The driver is connected to the laser diode by a transmission line, a so called stripline. For collimation and shaping of the output beam aspherical and cylindrical lenses are used. Then, it is coupled into a single mode fibre which can be connected to the main experiment.

5.2.1 Connection of the driver to the diode

As a conduction of short pulses (with rising/ falling slope on the order of nanoseconds) from the driver to the laser diode is needed, one has to make sure that the impedance of the connection between driver and diode is matched with the resistance of the diode in order to avoid reflections. This can be solved by making a micro stripline which is built of two stripes of copper separated by a stripe of polyamide (see fig. 5.3)[46].
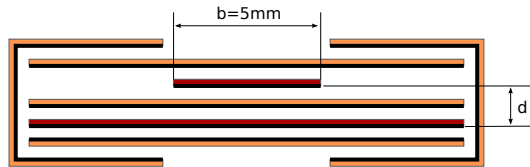

Figure 5.3: Schematic of the stripline. The copper stripes are drawn in red, the polyamide in orange and the glue in black.

The upper copper stripe is narrower than the lower one. By adjusting the width b of the upper stripe and the distance d the impedance can be tuned. The stripline was designed for the multi-mode diode which has a resistance of 5 Ω at 2 W optical output power.

If $\frac{b}{d} > 1$, one can approximate the impedance of the stripline by [46]:

$$Z_{L_s} = \frac{\frac{120\pi}{\sqrt{\epsilon_r}}}{\frac{b}{d}} \tag{5.1}$$

where ϵ_r = 3,5 is the dielectric constant of polyamide. An exact calculation is not possible as the dielectric constant of the glue is not known. Striplines with b = 5 mm were fabricated and turned out to work well, i.e. no current reflection effects were observed in the optical output signal. The same stripline also worked for the single-mode diode even though it has a ten times higher resistance than the multi-mode diode.

5.3 Optical setup

Optical Output Pulses of the Diodes

The optical pulses of the diodes are measured with a photodiode[4]. While the pulses of the single-mode diode look almost rectangular (see fig. 5.4), the multi-mode diode exhibits modulations in the amplitude of approximately 10 % and the edges are not as steep as the ones of the single-mode diode pulses.
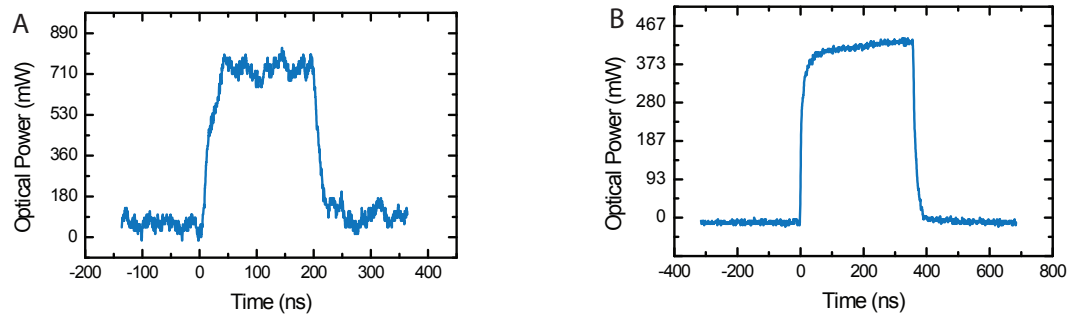

Figure 5.4: Optical output pulses of the multi-mode (A) and the single-mode (B) diode

5.3.1 Collimation and Shaping of the Beam

The aim is to couple as much power as possible to a single-mode fibre in order to be able to use the diode laser in the main experiment. To achieve a good coupling efficiency, the mode of the beam has to match with the mode of the fibre. A fibre with cut-off wavelength below 400 nm was chosen[5]. It has a mode field diameter of 2.9 μm (at 460 nm). In order to match the waist, several optical elements are used to collimate the beam, to correct for different divergence angles and for astigmatism.

---

[4]DET10A, Thorlabs
[5]405HP, APC, Thorlabs

51

Beam profile

The beam profile is measured with a CCD-camera[6]

a) Multi-Mode Diode   Figure 5.6, A and B show the profile of the multi-mode diode. Picture A was taken directly behind the collimation tube and picture B at a distance of approx. 40 cm. The beam was collimated along one axis with an aspherical lens of f = 4 cm[7] which was mounted in the collimation tube. The diode showed strong astigmatism so that it was not possible to collimate the beam in the two axis with one single lens. The beam was horizontally collimated by the lens in the collimation tube. In the vertical axis, the beam had a focus approx. 30 cm away from the source. In order to collimate the beam vertically, a cylindrical lens of f = 100 mm was mounted 10 cm behind the focus (see fig. 5.5).
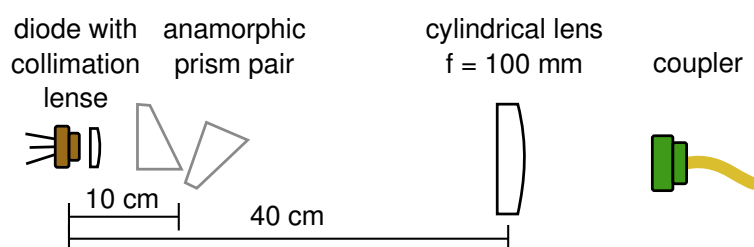

Figure 5.5: Optical elements used to shape the beam of the multi-mode diode. The anamorphic prism pair is not used in the final setup.

The profile of the beam directly behind the collimation tube looks like a $TEM_{1,0}$ mode. At larger distances, however, it behaves like a higher order mode (see fig. 5.6, C and D, taken at a distance of 1 m) and changes its orientation, i.e. its horizontal extension becomes larger than the vertical one.

The multi-mode diode has different divergence angles along the horizontal and vertical axes (see table 5.1). This has the effect that the collimated beam has different diameters in both axes. To compensate this effect, a prism pair is installed at 10 cm from the source

---

[6]Dataray
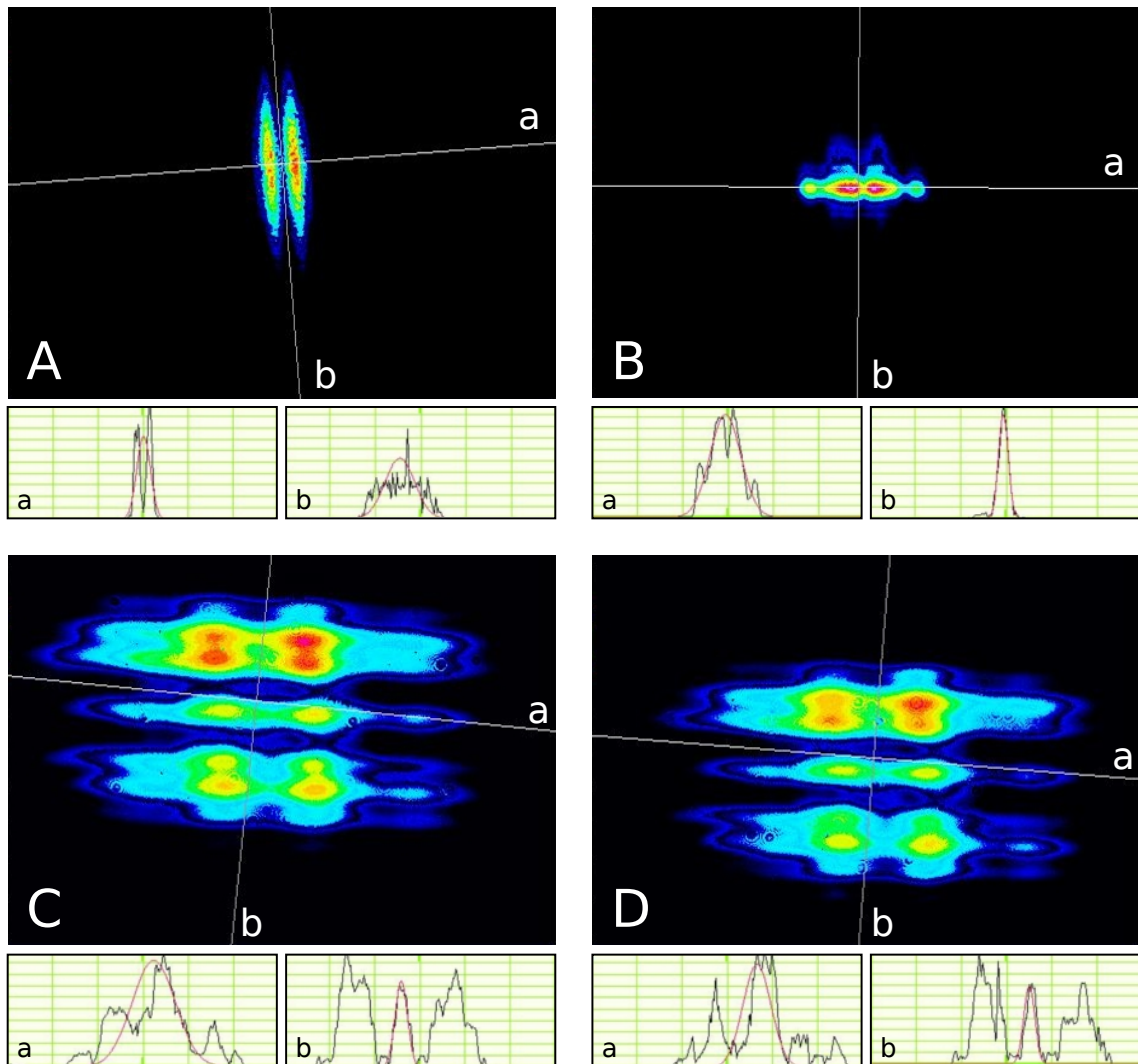[7]C610TME-A, Thorlabs

Figure 5.6: The beam profile of the 445 nm Nichia multi-mode diode. The beam is horizontally collimated. The picture shows the intensity distribution. A: directly behind collimation tube, B: in a distance of approx. 40 cm, C: in a distance of approx. 1 m including only cylindrical lens, D: in a distance of approx. 1 m including cylindrical lens and anamorphic prism pair

in order to narrow the beam along the horizontal axis. It turned out, however, that it is impossible to find a position where the beam keeps its circular shape at further distances. The prism pair does not notably change the mode (see fig. 5.6, D). For those reasons, the prism pair is not used any more.

b) Single-Mode Diode   The profile of the Nichia 445 nm single-mode diode comes close to the desired $TEM_{0,0}$ Gaussian (see fig. 5.8). Its astigmatism is low so that one single collimation lens is sufficient, but the different divergence angles were similar to the beam of the multi-mode diode. There were two different aspheric lenses available for the collimation of the beam with f = 4 mm (design wave length 408 nm)[8] and f = 4.02 mm (design wave length 410 nm)[9]. The profiles differed regardless of the similar specifications (see fig. 5.8, The diode was rotated by 90 ° between the two pictures). The profile with the lens of f = 4 mm looks as if the outer part of the beam is cut off although both lenses have an NA of 0.6. To exclude the possibility that this cut-off is caused by an improper centring or tilting of the diode, the diode was taken out and put back in a rotated position. As this did not change the pattern and a different diode by Osram[10] also showed the cut-off with the 4 mm lens, it can be assumed that it is a property of the lens itself. For the rest of this work, the collimation lens with f = 4.03 mm is used as it does not show such a cut-off at the edges. The collimated beam has waists of $w_0^{(x)} = 680$ μm and $w_0^{(y)} = 1379$ μm.

The first approach to obtain a more symmetrical beam was to use an anamorphic prism pair in order to diminish the larger waist ($w_0^{(y)}$) to half of its size (see fig. 5.7). It is possible to achieve a quite symmetrical beam (see fig. 5.9 (A, B)), but unfortunately the anamorphic prism pair did not only change the beam in the direction it was supposed to do so, but also a bit in the other one. For this reasons, a telescope of cylindrical lenses was set up which narrows the beam in y-direction by a factor of 2 (see fig. 5.9 (C, D)). For this purpose a pair of cylindrical lenses of f = -50 mm and f = 100 mm was used. The beam profile is similar to the one obtained with the prism pair (5.9 (A, B)).

---

[8]C610TME-A, Thorlabs
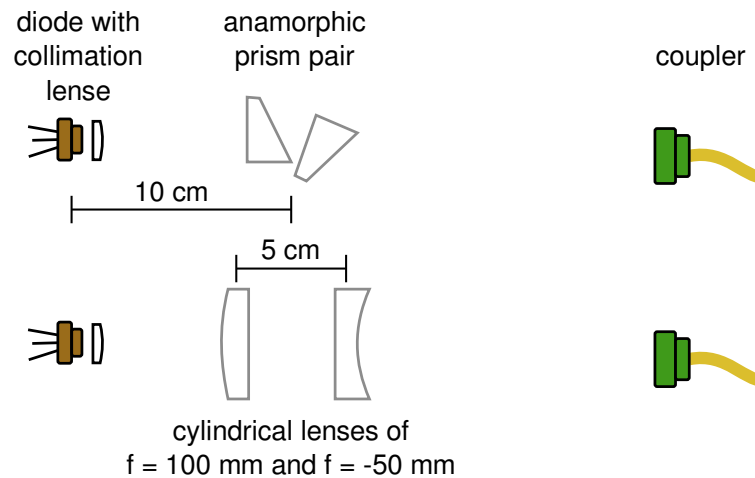[9]C671TME-A, Thorlabs
[10]PL T4 NSB

Figure 5.7: Optical elements used to shape the beam of the single-mode diode. Neither the anamorphic prism pair nor the microscope with cylindrical lenses is used in the final setup.

Close to the diode, the beam has a Gaussian shape with a sharp peak near its centre. At larger distances, this peak dominates the profile resembling a Gaussian shape. This makes it difficult to collimate, since one does not know how much one can rely on the fits of a Gaussian into the profile.

5.3.2 Coupling efficiencies

The shape of the pulses behind a single-mode optical fibre can be seen in fig. 5.10. The modulation of the amplitude of the pulse generated by the multi-mode diode are smaller at the output of the fibre than at its input (compare with fig. 5.4).

a) Multi Mode Diode   For the higher order output mode of the diode, only a low coupling efficiency into a single-mode fibre can be expected. For its maximisation, the available parameters are collimation, focussing and beam shape. A fibre-coupler by Schäfter und Kirchhoff with a lens of 11 mm[11] was used to couple the beam into the 450HP fibre from Thorlabs. A coupling efficiency of 6.6 % was achieved.

---

[11]60FC-4-A11-01
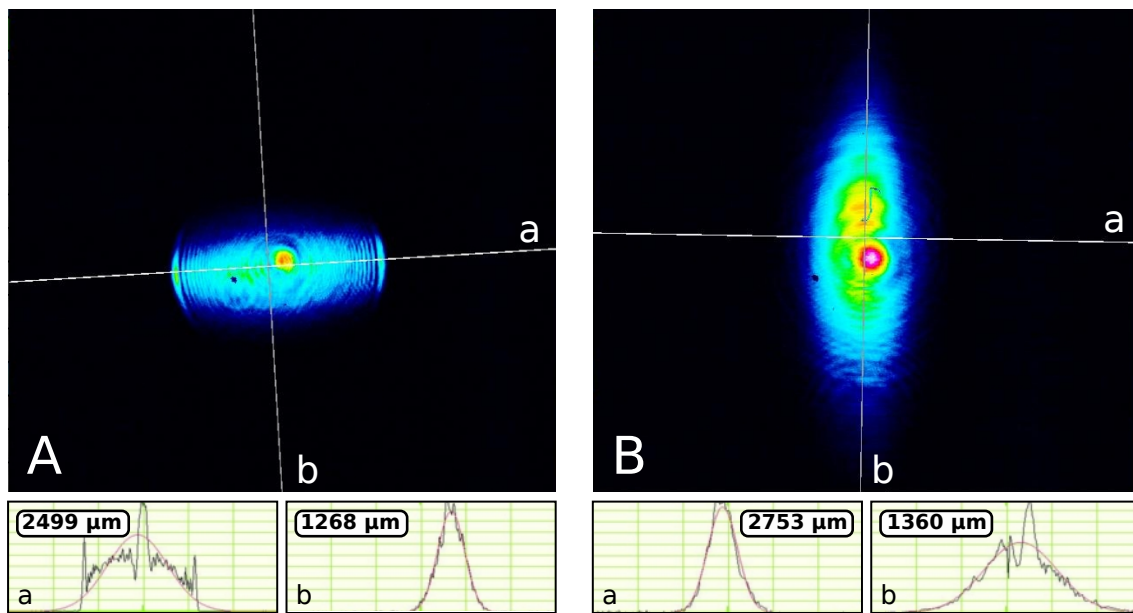
Figure 5.8: The beam profile of the 445 nm Nichia single-mode diode. The figure shows the intensity distribution and fits of Gaussians at the cross sections marked by the lines (a) and (b) as well as the diameter of the beam according to the fit. The two pictures have been taken at a distance of 10 cm (A) and 30 cm (B), respectively, and had been collimated by a lens with focal length f = 4 mm (A) and f = 4.02 mm (B) (The diode was rotated by 90 ° between the two pictures.)

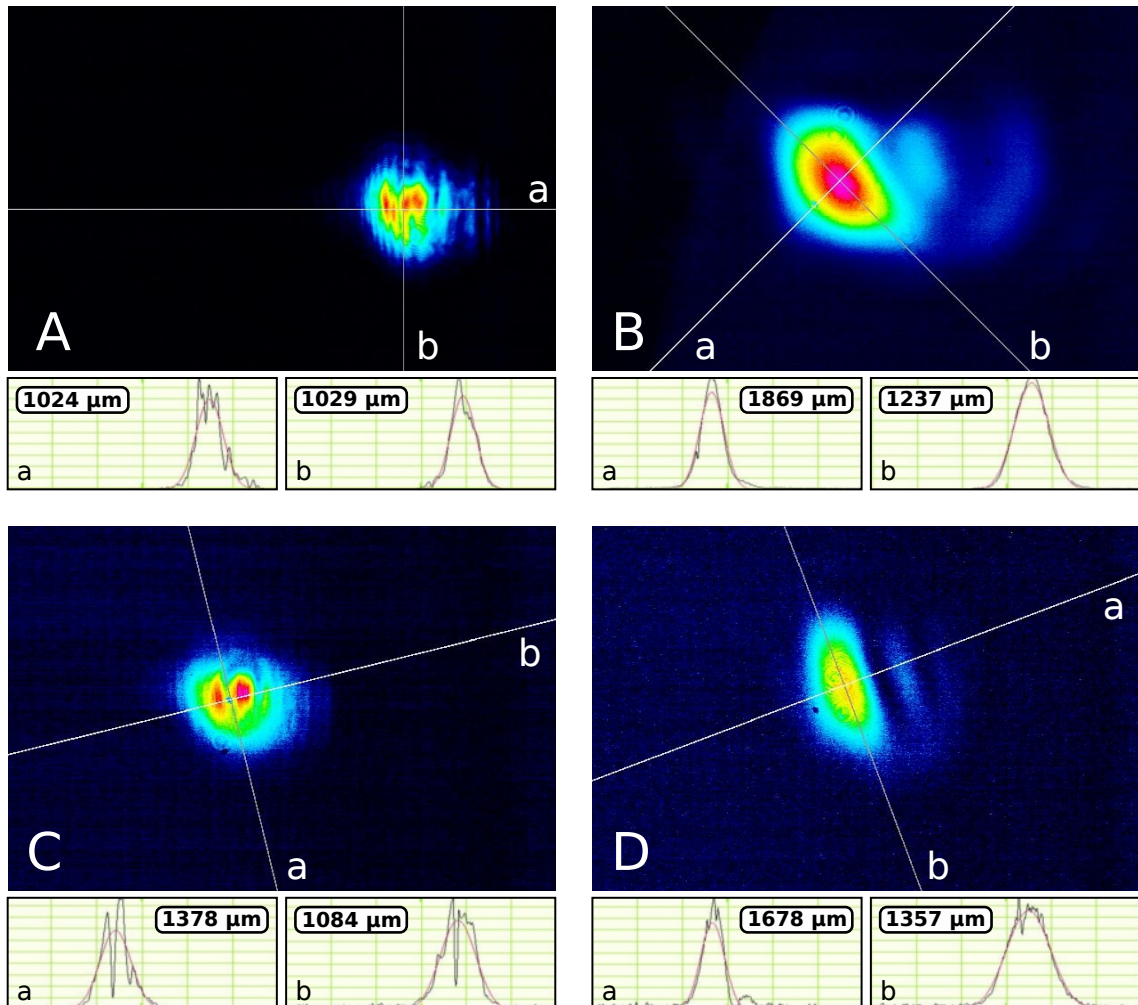Figure 5.9: The beam profile of the 445 nm Nichia single-mode diode measured 20 cm (A, C) and 1.5 m (B, D) away from the diode.The picture shows the intensity distribution and fits of Gaussians at the cross sections marked by the lines (a) and (b) as well as the diameter of the beam according to the fit. In A, B an anamorphic prism pair is used and in C, D a telescope with cylindrical lenses.
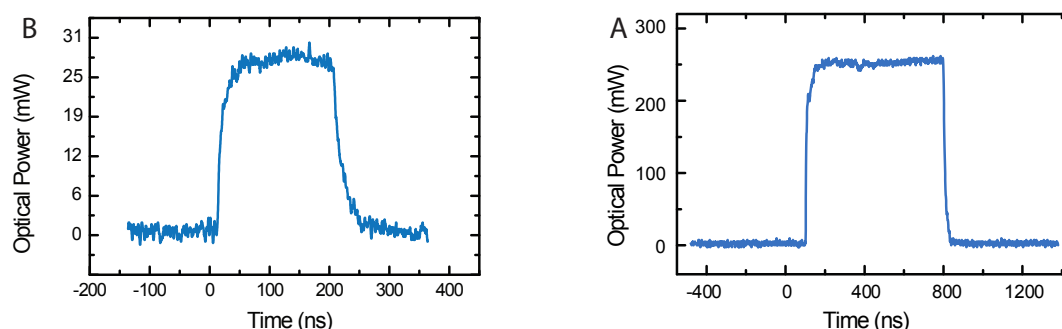
Figure 5.10: Pulses of the multi-mode (A) and single-mode (B) diode measured at the output of an optical single-mode fibre.

b) Single Mode Diode Using the anamorphic prism pair or the microscope with cylindrical lenses improve the beam profile and therewith the bare coupling efficiency. Unfortunately, their improvements are counteracted by losses at the optical components. It turned out that the best total coupling efficiency was achieved by only using a collimation lens and a lens to focus the beam on the fibre. For the single-mode diode, a fibre-coupler by Schäfter und Kirchhoff of 8.1 mm[12] and the same fibre (405HP, APC, Thorlabs) were used. The best achievable overall coupling efficiency was 62 %.

5.3.3 Operating the Laser Diodes at higher Currents

The main aim of the diode laser is to provide as much power as possible for the ionisation of ^{87}Rb . When the laser is used in the experiment for ionising atoms, pulses of several hundred nanoseconds are required every time the state of an atom is read out, this means at a low repetition rate of maximally 100 Hz. When testing the diodes, 300 ns to 700 ns-pulses at 50 Hz were used, i.e. a duty-cycle of about 25 ppm. Therefore thermal effects are not likely to destroy the laser diode when applying more current to the diode than it is specified for.

a) Multi-Mode Diode Applying 2 A, i.e. twice the specified current, to the multi-

---

[12]60FC-4-M8-33

mode diode, an optical output of 1.6 W is obtained. No degeneration of the diode could be observed over a period of half a year use in the state read-out in the main experiment.

When operating the multi-mode diode at a higher current than specified, a modulation of the amplitude of up to fifty percent can be observed after coupling to an optical single-mode fibre. This modulation depends strongly on the coupling and the higher the coupling efficiency, the stronger the modulations. Fig. 5.11 shows an example of pulses after the single-mode fibre. While A is a relative flat pulse, B (measured at maximum coupling efficiency) shows a strong modulation. Our assumption is that this behaviour is due to interference of higher order modes which are overlapped in the fibre.
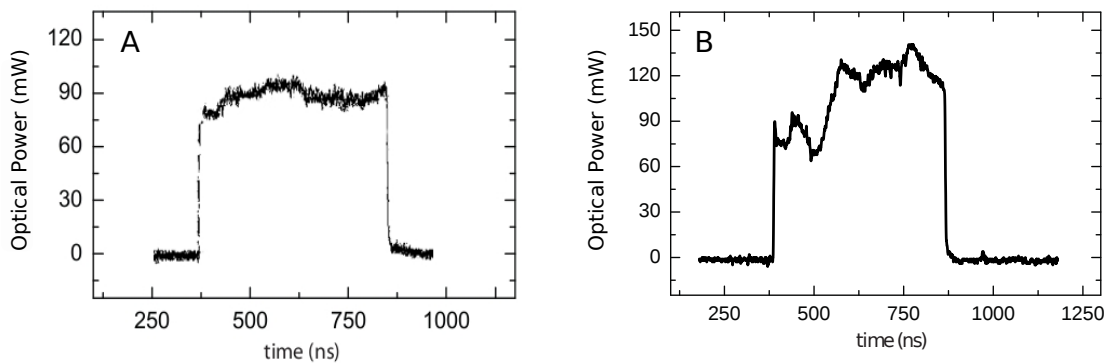
Figure 5.11: Pulses of the multi-mode diode behind an optical single-mode fibre when applying more current than it is specified for.

b) Single-Mode Diode   With the single-mode diode, the driver allows to go even further: By applying a current of 420 mA (4.2 times the specification), an output power of 420 mA was achieved without a change in the pulse shape. Above 450 mA higher order modes showed up which was visible as a modulation in the pulse shape, similar to 5.11.

For the applications, flat, rectangular pulses are desirable as variations of the intensity also cause variations in the light shift of the atomic states.

Achievable Output Powers after the Fibre

Table 5.2 gives a summary of the maximum output powers obtained after the fibre when the diodes were operating at more current than they were specified for.

Multi-mode diode		
flat pulse (fig. 5.11), A	90 mW	
maximal coupling (fig. 5.11), B	145 mW	at maximum
	70 mW	at minimum
	105 mW	on average
Single-mode diode		
maximal coupling	260 mW	

Table 5.2: Maximal powers achieved behind a single-mode fibre

5.4 Conclusion

5.4.1 Comparison to the previously used Laser System

Before the diode laser was set up, a diode-pumped frequency-doubled solid state laser at the wavelength of 473 nm and an output power of 350 mW had been used ([2], [47]). Short pulses needed for ionisation were realized by using an acousto-optic-modulator (AOM) [24]. After the passage through the AOM and coupling the light into a single-mode optical fibre, a power of 55 mW could be obtained behind the optical fibre [48].

5.4.2 Summary

The new diode laser turned out to be a good and inexpensive alternative to the so far used solid state laser as it provides up to 4.7 times the power the solid state laser setup did. Concerning the shaping of the beam, it was best to use as few optical components as possible because most of the time the loss of power by reflections was bigger than the gain achieved by a better beam profile. The single-mode diode has shown the best performance, because of the high output power and flat, rectangular pulses. This system

has been operating without degradation for a period of more than half a year. It is compact and optically as well as electrically compatible with the main experiment so that it is well suited for an integration in it.

6 Experimental Determination of the Ionisation Rate of Single ^{87}Rb Atoms

The new pulsed diode laser described in chapter 5 is integrated into the main experiment. Now, measurements of the ionisation time can be carried out and be compared to the previously used laser system. The ionisation rates at different powers of the ionisation laser can also be compared to theoretical predictions. This chapter describes a method to determine the ionisation rate and discusses the results.

6.1 Installation of the New Laser in the main Experiment

The new laser is integrated in the experiment by coupling it into the fibre which goes to the microscope set up.

As the wavelength of the formerly used laser was 473 nm and the new one is 450 nm, the focus of the beam is now shifted with respect to the atomic trap due to chromatic abberation of the objective. This shift is corrected for by adjusting the collimation by minimizing the ionisation time which is measured as follows:

6.2 Experimental Procedure to Determine Γ_{ion}

The ionisation rate is determined for a two step ionisation process starting from the $5^2S_{1/2}$, $F = 2$ state. The atom is prepared in this state by optical pumping using the
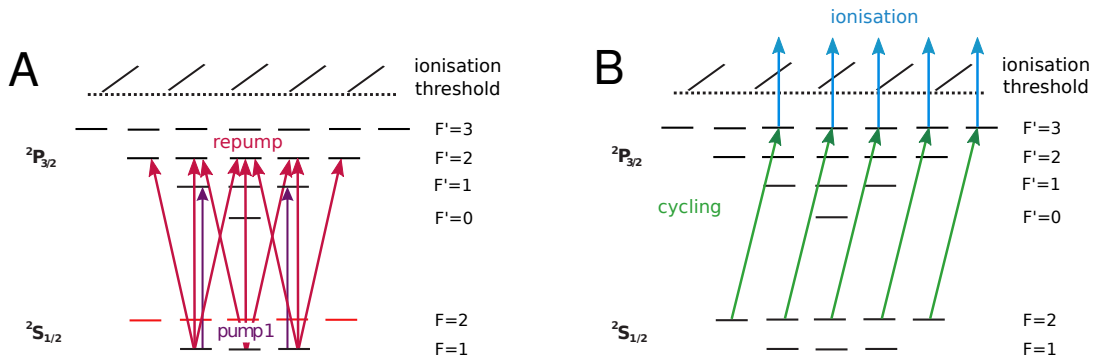
Figure 6.1: Pumping and two-step ionisation. A: The atom is pumped to to state $5^2S_{1/2}$, $F = 2$. B: Ionisation using the cycling and the ionisation laser.

pump 1 and the repump laser (see fig. 6.1, A). Afterwards the atom is excited by the cycling laser to the intermediate state $5^2P_{3/2}$, $F' = 3$ from where it can be ionised by the ionisation laser (see fig. 6.1, B). In order to detect, if the atom has been ionised (and has therewith left the trap), the cooling light is turned on as its fluorescence level shows if the atom is in the trap.

Figure 6.2: Variation of the pulse length of the cycling laser for the measurement of the ionisation time

The time the cycling laser is turned on determines the time the ionisation process can take place. Varying the length of the cycling pulses (see fig. 6.2) provides thus a method to measure the probability for a single atom to be ionised in a certain time. This procedure

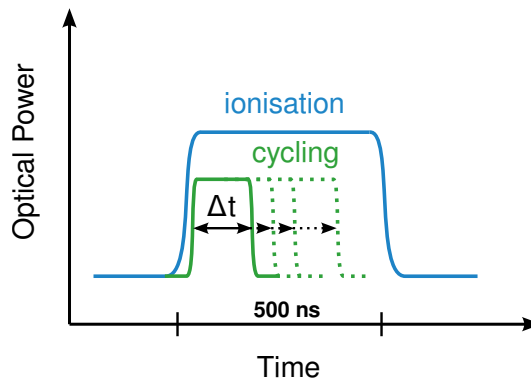is repeated several hundred to several thousand times. Plotting the measured ionisation probability against the pulse length of the cycling laser allows to determine the ionisation time τ' which is the time, in which the atom is ionised with the probability of $1-\frac{1}{e}$. In this measurement, the cycling laser is operated at 335 times the saturation intensity so that it drives many Rabi cycles during one pulse. Therefore, the population of the excited level approaches 50 % on average and the ionisation rate is given by:

$$\Gamma_{ion} = \frac{2}{\tau'}. \tag{6.1}$$

6.3 Results

For two different output powers of the ionisation laser, the probability to ionise an atom is measured varying the length of the cycling laser pulse. An exponential function $a + b \cdot e^{\frac{t}{\tau'}}$ is fitted to the measured data.

For a power of 90 mW after the single-mode fibre, a least square fit determines $\tau' = 41.6 \pm 0.9$ ns (see fig. 6.3, A).
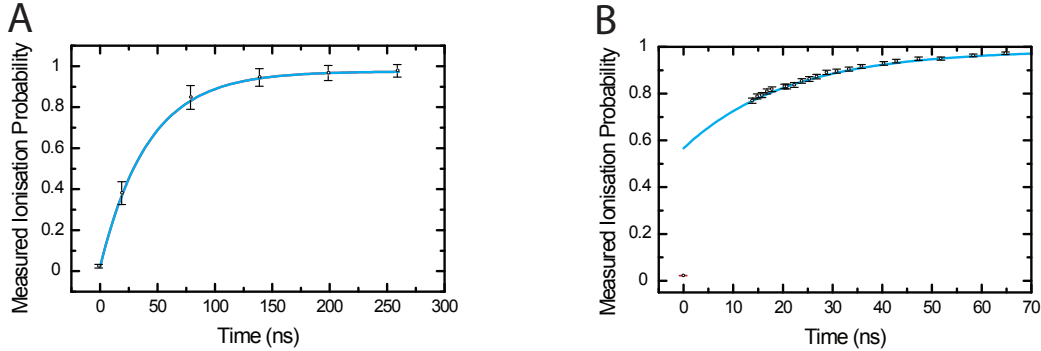

Figure 6.3: Measurement of the ionisation probability using an ionisation laser of 90 mW (A) and 260 mW (B)

For an output power of 260 mW a problem appears because it is not possible to generate pulses of less than 14 ns (FWHM) by switching the cycling pulses with our AOMs as the

pulses have rising/ falling edges of approximately this duration. The first point (in red) of the measured data (see 6.3, B), which was taken without any cycling pulse, obviously does not match with the rest of the data. To estimate a time constant, an exponential function is plotted to the data excluding this point. The fit does not predict an ionisation probability of zero for no cycling pulse, but at -18 ns. This shows, that the FWHM, which is used for the duration of the pulses, is not a good measure for such short pulses. A better measure could be the square root of the pulse area.

A least square fit to the data yields $\tau' = 21.1 \pm 1.1$ ns.

Another source of errors when measuring the ionisation time is, that the intensity of the ionisation laser at the atom depends strongly on the overlap of the ionisation laser with the dipole trap. Before each measurement, the overlap of both beams was checked at two different points, one of them some centimetres away from the trap and the second one at a distance of approx. 2 m. It can be adjusted to $\frac{1}{10}$ of the diameter of the beam. In a Gaussian beam, the intensity distribution is given by [50]:

$$I(r,z) = I_0 \left(\frac{w_0}{w(z)} \right)^2 \cdot e^{\frac{-2r^2}{w(z)^2}} \tag{6.2}$$

where z is the direction of the beam propagation, r the distance from the symmetry axis of the beam orthogonal to z, w_o the waist of the beam at the focus and w(z) at the distance z.

A deviation of the overlap by $\frac{1}{5w_0}$ therefore introduces a relative systematic error of the intensity at the atom of -7.7 % as:

$$\frac{I(r = \frac{w_0}{5}, z = 0)}{I_0} = e^{\frac{-2}{25}} = 0,923 \tag{6.3}$$

As $\tau' \sim \frac{1}{\Gamma} \sim \frac{1}{I}$, the resulting relative systematic error on τ' is equal to +7.7 %.

The results of the ionisation time τ' for the two different ionisation laser powers, including the error from an improper overlap are summarised in 6.1

	90 mW	260 mW
τ' (ns)	41.6 (+ 0.9 - 4.1)	21.1 (+ 1.1 - 2.7)

Table 6.1: Experimentally determined time constants τ' for the ionisation from the $5^2S_{1/2}$, $F = 2$ level.

Comparison to the Previously used Laser and to Theory

The formerly used solid state laser had an output power of 55 mW [48] and a time constant of $\tau' = 64.4 \pm 2.8$ ns [2].

Theory predicts, that the ionisation rate depends linearly on the intensity of the laser beam (see chapter 4.1):

$$\Gamma_{if}(\omega_\gamma, I_\gamma) = \frac{\sigma_\gamma(\omega_\gamma)}{\hbar\omega_\gamma}I_\gamma \qquad (6.4)$$

An estimation can be done using the average of the measured cross section (Eq: 4.4): $\Gamma_{if}(\omega_\gamma, I_\gamma) = 1.0438 \cdot 10^9 \frac{1}{sW} P$.

In order to compare the measured data with the theoretical estimation, losses of the power of the ionisation laser at the optics of the microscope of 40 % [49] have to be considered. Furthermore, it is assumed that the wave length dependence of the waist can be neglected. Picture 6.4 shows the ionisation rate dependence of the three measured points and the line represents the prediction of the theoretical estimation. The ionisation rate is given in multiples of the total decay rate of the D_1 transition (2π $5.756 \cdot 10^6 \frac{1}{s}$).

The first two measured points coincidence with the theoretical estimation, but the third one deviates strongly from the prediction. This shows clearly that the error of the fit underestimates the real error due to a not well defined pulse length of the cycling laser which becomes most obvious when using short pulses.

For very short pulses, another effect becomes important. The Rabi frequency is given by [1]:
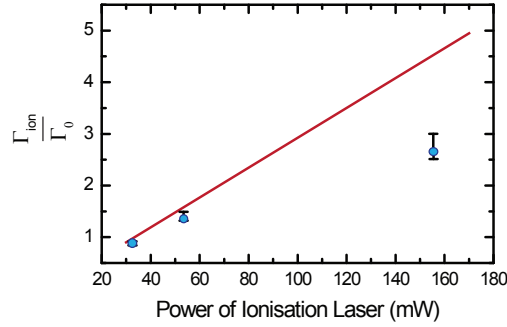
Figure 6.4: The three points represent the measurements of the ionisation rate at $P = 0.6 \cdot 55$ mW, $P = 0.6 \cdot 90$ mW and $P = 0.6 \cdot 250$ mW (including the losses of 40 %). The red line shows the theoretical estimation.

$$\Omega = \Gamma \sqrt{\frac{I}{I_{sat}}} \qquad (6.5)$$

For the cycling laser being used at 335 times the saturation frequency, a duration of 2 ns for a Rabi cycle is obtained. In the limit of pulses of this duration, the approximation of a population of $\frac{1}{2}$ of the excited state is not valid any more.

6.4 Conclusion

In this chapter, experimental measurements of the ionisation rates of single ^{87}Rb atom is presented. Ionisation rates of $\Gamma(90mW) = 1.33$ (+ 0.03 - 0.13) Γ_0 and $\Gamma(260mW) = 2.63$ (+ 0.14 - 0.34) Γ_0 was obtained. Especially in the second measurement, the error is underestimated as short pulses are used in the measurement which are limited by the rising/ falling edge of the pulse. The theoretical estimation coincides well with the first ionisation time, but predicts a considerably higher value for the second power. In order to get a better result for the ionisation rate at 260 mW, shorter pulses have to be used which can be generated for example by an EOM [24]. On the scale of very short pulses, a step-like behaviour of the measured ionisation probability might be visible. These steps are caused by the Rabi cycles of the cycling laser: The ionisation probability depends on where in the Rabi cycle one stops the excitation by the cycling laser.

7 Summary and Outlook

The aim of this thesis was to prepare the main experiment for atom-atom entanglement by making calibration measurements as well to improve the detection process of the atoms by building a new laser and making calculations on a new detection scheme.

In the first part of this thesis, an overview of the main experiment is given. Then follows a description of calibration measurements made at setup 2 with the objective of improving the contrast of atom-photon entanglement, as well as the connection and the synchronisation of the excitation procedures of the two setups. For this purpose, magnetic fields were compensated in order to avoid a Larmor precession of the spin state of our qubit. A Larmor period well above 200 μs could be achieved, which ensured that the spin-state did not change during the detection process. Together with the calibration of the polarisation of the laser which determines the atomic measurement basis, a visibility of entanglement between atom and photon of more than 90 % was achieved.

The mechanical stability of the experiment was improved, which guaranteed a stable connection between the two atomic traps. Furthermore, the wavepackets of the spontaneously emitted photons were overlapped. This allowed us to generate entanglement between remote atoms with a visibility of more than 0.707, the value which is necessary to violate Bell's inequality. In order to close the locality and the detection loophole when making spin state measurements on remote entangled atoms, a fast, efficient state read-out as well as separation by a larger distance is necessary.

The central part of the thesis is about fast spin-state selective detection of ^{87}Rb atoms by ionisation. This is not only an important requirement for the spacelike separation of the two measurements on the atoms in a future loophole free test of Bell's inequality, but also is an important tool for fundamental research in quantum optics and atomic physics

and can have applications in quantum communication.

To enable a fast ionisation process, a new pulsed diode laser of 450 nm was set up and different laser diodes were tested. The single-mode diode by Nichia showed the best performance and provided up to 260 mW after coupling to a single mode fibre. Therewith, the new diode laser can provide up to 4.7 times the optical output power of the previously used solid state laser system after couping to a single-mode fibre. The design of the diode laser allows one to easily exchange the diode once there are more powerful diodes available at a similar wavelength.

The ionisation rate was measured for two different powers of the ionisation laser. The best ionisation rate was 2.63 (+ 0.34 - 0.14) Γ_0. In order to determine this constant more accurately, a tool to generate shorter pulses, e.g. an EOM, would be necessary.

Such a short ionisation time allows for a new and faster scheme using direct ionisation. Calculation for this scheme has been carried out. Compared to the scheme used so far which includes a STIRAP transition, the detection by ionisation is faster for higher powers of the ionisation laser, although for the power provided now, calculations predict that the STIRAP scheme still works better. However, it is expected to obtain a comparable contrast of the total detection within 300 ns, which, yet, has to be experimentally tested first.

Using a fast, efficient method to detect the ionisation fragments, e.g. channel electron multipliers [2], a state read-out with a fidelity above 97 % within 1 μs should be possible with the new laser and the new detection scheme. This can be used not only for single site resolved detection of the atomic state, but also can help to close the locality loophole in a future loophole-free test of Bell's inequality.

Bibliography

[1] H. J. Metcalf, P. van der Straten. *Laser cooling and trapping*. Springer Verlag, New York, 1999

[2] F. Henkel, M. Krug, J. Hoffmann, W. Rosenfeld, M. Weber, H. Weinfurter. *Highly Efficient State-Selective Submicrosecond Photoionisation Detection of Single Atoms*. Phys. Rev. Lett. 105,253001, 2010

[3] K. D. Nelson, X. Li, D. S. Weiss. *Imaging single atoms in a three-dimensional array*. Nature Physics 3,556-560, 2007

[4] T. Gericke, P. Würtz, D. Reitz, T. Langen, H. Ott. *High-resolution scanning electron microscopy of an ultracold quantum gas*. Nature Physics 4,949-953, 2008

[5] M. Karski, L. Förster, J. M. Choi, W. Alt, A. Widera, and D. Meschede. *Nearest-Neighbor Detection of Atoms in a 1D Optical Lattice by Fluorescence Imaging*. Phys. Rev. Lett. 102,05300,1 2009

[6] W. S. Bakr, J. I. Gillen, A. Peng, S. Fölling, M. Greiner. *A quantum gas microscope for detecting single atoms in a Hubbard-regime optical lattice*. Nature 462,74-77, 2009

[7] J. F. Sherson, C. Weitenberg, M. Endres, M. Cheneau, I. Bloch, S. Kuhr. *Single-atom-resolved fluorescence imaging of an atomic Mott insulator*. Nature 462,74-77, 2009

[8] A. Einstein, B. Podolsky, and N. Rosen. *Can quantum-mechanical description of physical reality be considered complete?*. Phys. Rev., 47,777780, 1935

[9] Erwin Schrödinger. *Die gegenwärtige Situation in der Quantenmechanik*. Die Naturwissenschaften, Volume 23, Number 48, 807-812, 1935

[10] J. S. Bell. *On the Einstein-Podolsky-Rosen paradox*. Physics, 1,195, 1964

[11] J. F. Clauser, M. A. Horne, A. Shimony, and R. A. Holt. *Proposed experiment to test local hidden-variable theories*. Phys. Rev. Lett., 23,880884, 1969

[12] S. J. Freedman, J. F. Clauser. *Experimental test of local hidden-variable theories*. Phys. Rev. Lett. 28,938941, 1972

[13] J. F. Clauser, A. Shimony. *Bell's theorem: experimental tests and implications*. Rep. Prog. Phys. 41,1881, 1978

[14] A. Aspect, P. Grangier, G. Roger. *Experimental tests of realistic local theories via Bell's theorem*. Phys. Rev. Lett. 47,460-463, 1981

[15] A. Aspect, P. Grangier, G. Roger. *Experimental realisation of Einstein-Podolski-Rosen-Bohm Gedankenexperiment: A new violation of Bell's inequality*. Phys. Rev. Lett. 49,91-94, 1982

[16] A. Aspect, J. Dalibard, G. Roger. *Experimental test of Bell's inequality using time-varying analyser*. Phys. Rev. Lett. 49,1804-1807, 1982

[17] G. Weihs, T. Jennewein, C. Simon, H. Weinfurter, A. Zeilinger. *Violation of Bell's inequality under strict Einstein locality conditions*. Phys. Rev. Lett., 81,5039-5043, 1998

[18] M. A. Rowe, D. Kielpinsky, V. Meyer, C.A. Sacket, W. M. Itano, C. Monroe, D.J. Wineland. *Experimental violation of Bell's inequality with efficient detection*. Nature, 409,791-794, 2001

[19] P.M. Pearle. *Hidden-Variable Example Based upon Data Rejection*. Phys. Rev. Lett. D, 2,14181425, 1970

[20] A. Garg, N.D. Mermin. *Detector inefficiencies in the Einstein-Podolsky-Rosen experiment*. Phys. Rev. Lett. D, 35,38313835, 1987

[21] M. Zukowski, A. Zeilinger, M. A. Horne, A. K. Ekert. *"Event-ready-detectors" Bell experiment via entanglement swapping* Phys. Rev. Lett. 71,42874290, 1993

[22] W. Rosenfeld, M. Weber, J. Volz, F. Henkel, M. Krug, A. Cabello, M. Zukowski, H. Weinfurter. *Towards a Loophole-Free Test of Bell's Inequality with Entangled Pairs of Neutral Atoms.* Advanced Science Letters 2,469-474, 2009

[23] N. Schlosser, G. Reymond, P. Grangier. *Collisional blockade in microscopic optical dipole traps.* Phys. Rev. Lett. 89,230051-230055, 1998

[24] Michael Bass et. al. *Handbook of Optics, Volume II.* McGraw-Hill, 1995

[25] J. Volz, M. Weber, D. Schlenk, W. Rosenfeld, J. Vrana, K. Saucke, C. Kurtsiefer, H. Weinfurter. *Observation of Entanglement of a Single Photon with a Trapped Atom.* Phys. Rev. Lett. 96,030404, 2006

[26] M. Weber *Quantum optical experiments towards atom-photon entanglement* PhD thesis, Ludwig-Maximilians-Universität München, 2005

[27] J. Volz. *Atom-photon entanglement.* PhD thesis, Ludwig-Maximilians-Universität München, 2006

[28] K. Bergmann, H. Theuer, B. W. Shore. *Coherent population transfer among quantum states of atoms and molecules.* Rev. Mod. Phys. 70,10031025, 1998

[29] F. Vewinger, M. Heinz, R. G. Fernandez, N. V. Vitanov, K. Bergmann. *Creation and Measurement of a Coherent Superposition of Quantum States.* Phys. Rev. Lett. 91,213001, 2003

[30] F. Vewinger, M. Heinz, R. G. Fernandez, N. V. Vitanov, K. Bergmann. *Measurement of subpicosecond time intervals between two photons by interference.* Phys. Rev. Lett. 59,20442046, 1987

[31] M. Fürst, H. Weier, S. Nauerth, D. G. Marangon, C. Kurtsiefer, H. Weinfurter. *High speed optical quantum random number generation.* Opt. Express 18,13029-13037, 2010

[32] W. Rosenfeld. *Experiments with an Entangled System of a Single Atom and a Single Photon*. PhD thesis, Ludwig-Maximilians-Universität München, 2008

[33] N. Ortegel. *Atom-Photon Entanglement*. Diplomarbeit, Ludwig-Maximilians-Universität München, 2009

[34] E. Hecht. *Optics*. fourth edition, Addison Westley, 2002

[35] R. Ulrich, S.C. Rashleigh, and W. Eickhoff. *Bending-induced birefringence in single-mode fibers*. Opt. Lett. 5,273, 1980

[36] F. Hocke. *Long Distance Atom Photon Entanglement*. Diplomarbeit, Ludwig-Maximilians-Universität München, 2007

[37] V. S. Lethokhov. *Laser Photoionization Spectroscopy*. Academic Press Inc, 1987

[38] I. I. Sobelman. *Atomic Spectra and Radiative Transitions*. second edition, Springer Verlag, 1992

[39] M. Aymar, O. Robaux, S. Wane. *Central-field calculations of photoionisation cross sections of excited states of Rb and Sr$^+$ and analysis of photoionisation cross sections of excited alkali atoms using quantum defect theory*. J. Phys. B: At. Mol. Phys. 17,993, 1984

[40] C. Gabbanini, S. Gozzini, A. Lucchesini. *Photoionization cross section measurement in a Rb vapor cell trap*. Optics Communications, Volume 141, Issues 12, 1997

[41] T. P. Dinneen, C. D. Walace, K.-Y. N. Tan, P. L. Gould. *Use of trapped atoms to measure absolute photoionization cross sections*. Opt. Lett. 17,1708, 1992

[42] W. Huang, Y.-P. Ruan, F.-D. Jia, Y.-P. Zhong, L.-W. Liu, X.-C. Dai, P. Xue, X.-Y. Xu. *Measurement of the Absolute Photoionization Cross Section for the $5P_3/2$ State of ^{87}Rb in a Vapor Cell Magneto-optic Trap*. Chinese Phys. Lett. 29,013201, 2012

[43] J. Evers. *Light Matter Interactions*. Lecture at the Universität Heidelberg, 2010/2011

[44] Daniel A. Steck. *Rubidium 87 D Line Data*. Theoretical Division (T-8), Los Alamos National Laboratory

[45] L. Ricci, M. Weidemüller, T. Esslinger, A. Hemmerich, C. Zimmermann, V. Vuletic, W. König, T.W. Hänsch, *A compact grating-stabilized diode laser system for atomic physics* Optics Communications 117:541-549 (1995)

[46] Doc 9100-0232 Rev 1 Directed Energy Inc., 2003

[47] F. Henkel. *Photoionisation detection of single Rb-87 atoms using channel electron multipliers*. PhD thesis, Ludwig-Maximilians-Universität München, 2011

[48] Michael Krug. private communications, 2012

[49] C. Lee. *Observing Single Atoms*. Master thesis, Technische Universität München, 2011

[50] B. E. A. Saleh, M. C. Teich. *Fundamentals of Photonics*. second edition, Wiley, 2007

Danksagungen

An dieser Stelle möchte ich mich ganz herzlich bei allen bedanken, die zum Gelingen dieser Arbeit beigetragen haben, insbesondere:

- Professor Harald Weinfurter für die Aufnahme in seiner Arbeitsgruppe und die gute Arbeitsatmosphäre

- Professor Markus Oberthaler dafür, dass er meine Diplomarbeit von Heidelberg aus betreut hat

- Wenjamin für die Betreuung beim Aufbau des Ionisation-Lasers und für die vielen Erklärungen

- Michael für die Betreuung und Einführung in das Experiment und die schöne Zeit zusammen im Labor und auerhalb

- Norbert, Julian, Florian und Markus, an die ich mich immer bei Fragen wenden konnte

- Daniel S., der mir bei Problemen immer zur Seite stand

- Allen Mitglieder der Arbeitsgruppe Weinfurter für die gemeinsamen Mittagessen und die schöne Zeit zusammen

- Meiner Familie, ohne deren Unterstützung, sowohl moralisch als auch finanziell, mein Studium unmöglich gewesen wäre

- Marcos dafür, dass er mich immer unterstützt hat und immer für mich da war

- Meinen Freunden, die mich während meines Studiums begleitet haben

Erklärung:

Ich versichere, dass ich diese Arbeit selbstständig verfasst habe und keine anderen als die angegebenen Quellen und Hilfsmittel benutzt habe.

Heidelberg, den 05.04.2012 . . . .